THE FINITE ELEMENT METHOD IN LOW SPEED AERODYNAMICS

Final Technical Report
by
A.J. Baker
and
P.D. Manhardt

Prepared for the
NATIONAL AERONAUTICS AND SPACE ADMINISTRATION
LANGLEY RESEARCH CENTER
HAMPTON, VIRGINIA 23665

Under

NASA Grant NSG-1038

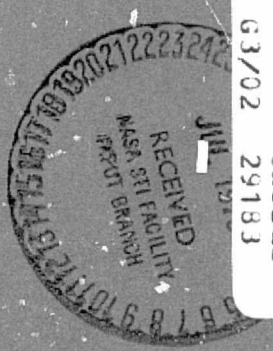

SCHOOL OF ENGINEERING
OLD DOMINION UNIVERSITY
NORFOLK, VIRGINIA

May 1975

Technical Report 75-T5

SCHOOL OF ENGINEERING
OLD DOMINION UNIVERSITY
NORFOLK, VIRGINIA

Technical Report 75-T5

THE FINITE ELEMENT METHOD IN LOW SPEED AERODYNAMICS

By

A.J. Baker

and

P.D. Manhardt

Prepared for the
National Aeronautics and Space Administration
Langley Research Center
Hampton, Virginia 23665

Under
Grant NSG 1038

Submitted by the
Old Dominion University Research Foundation
P.O. Box 6173
Norfolk, Virginia 23508

May 1975

TABLE OF CONTENTS

ILLUSTRATIONS

TABLES

THE FINITE ELEMENT METHOD IN LOW SPEED AERODYNAMICS

by

A. J. Baker
Visiting Professor*
Old Dominion University

and

Paul D. Manhardt
Textron Bell Aerospace

SUMMARY

Within recent years, the finite element method has emerged as an alternative theoretical foundation for establishing numerical solution algorithms for field problems in continuum mechanics, and in particular fluid dynamics. The fundamental concept of the finite element procedure is identification of a computational control-volume within which the conservation laws of mechanics are numerically approximated using a well-defined and uniformly consistent procedure. In contrast to the more familiar finite difference technique, the finite element algorithm explicitly retains use of the calculus and vector field theory in formation and evaluation of the discretized-equivalent matrix statement of control-volume conservation properties. For specifically non-linear differential equations, like the Navier-Stokes system in fluid dynamics,

*On leave from Textron Bell Aerospace, 1974-75 academic year.

the finite element method always yields a unique discretized-equivalent matrix expression. Interestingly, the resultant expressions appear uniformly comparable to the computationally preferred forms established via trial and evaluation techniques using difference algebra. These theoretical features, coupled with its intrinsic capability to employ specifiably non-regular computational meshes, and to enforce non-trivial gradient-type boundary conditions on non-coordinate solution domain boundaries, appears to render the finite element procedure of particular potential use in computational aerodynamics.

The results of a study, conducted for verification of this hypothesis and reported herein, indeed show that the finite element procedure can be of significant impact in design of the "computational wind tunnel" for low speed aerodynamics. The uniformity of the mathematical differential equation description, for viscous and/or inviscid, multi-dimensional subsonic flows about practical aerodynamic system configurations, is utilized to establish the general form of the finite element algorithm, universally applicable to all problem classes. The COMOC computer program, under development for several years as a finite element test bed, is similarly applicable to each of these diverse classes. Following completion of the theoretical developments, example numerical results for inviscid flow analyses, as well as viscous boundary-layer, parabolic- and full- Navier-Stokes flow descriptions, verify the capabilities and overall versatility of the fundamental algorithm for aerodynamics. The proven mathematical basis, coupled with the distinct user-orientation features of the computer program embodiment, portend near-term evolution of a highly useful analytical design tool to support computational configuration studies in low speed aerodynamics.

INTRODUCTION

Development of the technique, that has emerged as "the finite element method," began in the civil and structural engineering community in the early 1950's. Conventional engineering structures can be visualized as comprised of discrete elements interconnected at a finite number of points. For example, the analysis of pin-connected structures via imposition of a global force balance, can determine tension and compression members and loads; it is a well established study at the undergraduate level. In an elastic (or any other!) continuum, however, the number of such connections becomes infinite, and therein lies the difficulty in establishing a tractible engineering analysis. Turner et al. (ref. 1), in their original concept of a "finite element," attempted to bridge this gap by introducing a method to transform a continuum into an equivalent discretized finite assemblage of nodal behavior. The method developed rapidly thereafter, in good part due to the parallel development of large capacity digital computers. Existence of this computer hardware made possible the embodiment of the analytical developments into a viable tool (computer program) for engineering analysis of complex non-conventional structures.

While a detailed static force balance formed the theoretical foundation for the earlier finite element developments, this was rapidly replaced by the energy concepts that also form a significant branch of conventional structural analysis. From this viewpoint, the "finite element method" emerged as a technique for modeling the strain energy of a continuum structural system in terms of the behavior of local discrete subsystems. Total system energy is approximately determined by the assembly of the incremental work done by the surface tractions and imbedded stress distribution as the equivalent discretized structure is loaded. The actual node point displacement distribution is then determined by extremizing the strain energy integral with respect to the family of admissable displacement states; the physically realizable state corresponds to the energy minimum. Quite logically, these concepts were immediately recognized as belonging to the analytical theory of self-adjoint systems, the variational calculus and the theory of linear partial differential equations, as well as the corresponding principles in Hamiltonian mechanics including the Principle of Least Action and the Euler-Lagrange equations (cf., Goldstein

ref 2). Hence, the finite element method rapidly gained theoretical stature as well as practical usefulness, albeit at the cost of conceptual restriction to linear problems in mechanics.

In the mid-1960's, members of the engineering mechanics technical community, especially those with a background in mathematics or continuum mechanics but generally outside of structural mechanics, began to take note of the demonstrated power and versatility of the finite element procedure for analyzing complex problems. Particularly impressive was the ability of the algorithm to readily impose non-trivial (gradient) boundary condition constraints on irregularly shaped geometries, and to employ non-uniform discretizations of the problem solution domain (cf. Zienkiewicz, ref. 3). Each of these areas posed particular problems for more conventional numerical analysis procedures. Their apparent total alleviation by finite elements immediately prompted its extension to analyses of other linear field problems (cf. Zienkiewicz and Cheung, ref. 4) including steady heat conduction, and importantly subsonic potential flow. In this latter area, of our particular interest as a starting point, the differential equation is simply the linear Laplacian on the velocity perturbation potential function. However, the boundary conditions become specified on the behavior of its derivative normal to any surface, e.g., an airfoil, which in general is not parallel to a coordinate surface of the differential equation description. Because of the linearity, an energy-functional equivalent of the differential equation is readily established, including explicitly the non-trivial boundary condition statement. Using direct adaptation of structural computer code concepts, deVries and Norrie (ref. 5) obtained representative finite element solutions to two-dimensional aerodynamic flow in cascades using straightsided triangular elements. Computations for other two-dimensional aerodynamic configurations are given by Meissner (ref. 6); Sarpkaya and Hiriart (ref. 7) present results for an axisymmetric geometry involving a free surface of unknown location. Results using higher order finite element functionals, and curved-sided elements for improved geometric simulation, for two-dimensional potential flows are given by Thompson (ref. 8), Isaacs (ref. 9), and Hirsch and Warzee (ref. 10). The case for a specified freestream vorticity, "frozen" into an aerodynamic flow, is discussed by Vooren and Laburjere (ref. 11) using linear two-dimensional finite elements.

In all cases, the cited analyses correspond to the inviscid, steady, isoenergetic two-dimensional flow of an irrotational (or circulation preserving), incompressible fluid, i.e.,potential flow aerodynamics. However, current high-lift aerodynamic geometries employ complex combinations of flap and slat systems. Powered lift configurations, using engine exhaust and/or mass ejector systems, are areas of current aerodynamic research and development. All these flow fields depart significantly from linear potential flow, and viscous and/or turbulence effects form a large and important influence. Fortunately, interest in applying the finite element method of analysis to specifically non-linear flow fields was spawned in the late 1960's as well, with early attention focused on establishing an alternative theoretical foundation (since these problems did not appear self-adjoint!) The Method of Weighted Residuals was rediscovered (see Finlayson and Scriven, ref. 12), and emerged as a theoretical foundation for deriving finite element solution algorithms for arbitrarily non-linear partial differential equation systems. The linear potential flow case then became a special subclass of the more general formulation. Application to non-steady, two-dimensional aerodynamics is discussed by Bratanow and Ecer (ref. 13). Baker (ref. 14-16) presents numerous applications to a wide range of problems involving two- and three-dimensional viscous flows with turbulence and chemical reaction. Chan et al. (ref. 17) document extension of the finite element method to predictions in transonic aerodynamics.

These computational results provide demonstration (by parts) of the potential capabilities of the finite element method for analysis of complex aerodynamic systems. However, for the "computational wind tunnel" to become a truly viable alternative to extensive physical testing, it is imperative that the computer conduct a compleat analysis. To do so, the geometrical modeling must be performed with high fidelity, accounting of viscous/inviscid interaction must be intrinsic, and the inherent non-linearities of fluid mechanics must be accurately and economically captured by the computational mathematics. The two most important outputs from a computer study in aerodynamics are surface pressure distributions and overall drag; each can be accurately determined only by an adequate accounting for the entire physical system. Therefore, it is important to quantify the various flow disciplines, and to proceed through evaluation of the important analytical subsystems that constitute characterization of a realistic subsonic aerodynamic configuration.

This report documents results of a study conducted for this purpose on the subject NASA Grant under the sponsorship of the Low Speed Aerodynamics Branch, STAD, NASA Langley Research Center. By resorting to the fundamental mathematics, the differential equation systems appropriate for description of various aerodynamic flow regimes are derived. Their basic structure is noted: the underlying mathematical uniformity is utilized to subsequently establish the finite element solution algorithm applicable to all equation systems. The COMOC finite element computer program system, under development for analysis of problems in fluid and continuum mechanics, is briefly described. Subsequently, numerical results on finite element analysis of the various problem classes of impact in aerodynamics are presented, with discussion of factors affecting solution accuracy, speed and adequacy as well as user-orientation of the analysis procedures. A summary of results completes the report.

The work was primarily conducted while the senior author was on leave from Bell Aerospace Division of Textron as Visiting Associate Professor of Engineering Mechanics at Old Dominion University. We wish to acknowledge the long-term support given to research in finite element methods in fluid and continuum mechanics by Bell Aerospace, and the opportunity presented by Old Dominion University to carry out this work.

NOMENCLATURE

a	boundary condition coefficient; unit vector
A	area
b	coefficient; unit vector
B	body force
c	coefficient; speed of sound
c_p	specific heat
C	chord; coefficient
C_f	skin friction
D	binary diffusion coefficient
e	alternating tensor
E	symmetric velocity gradient
Ec	Eckert Number

f	function of known argument
Fr	Froude Number
g	function of known argument
h	static enthalpy; convection heat transfer coefficient
H	stagnation enthalpy
$\hat{i},\hat{j},\hat{k}$	unit vectors of rectangular Cartesian coordinate system
k	thermal conductivity; constant
K	generalized diffusion coefficient
ℓ	differential operator; turbulent mixing length
L	characteristic length; differential operator
Le	Lewis Number
M	Mach number; number of finite elements
n	unit normal vector; coordinate normal to a curve
p	pressure
Pr	Prandtl Number
q	generalized dependent variable
Q	heat addition; generalized discretized dependent variable
R	perfect gas constant; domain of elliptic operator
Re	Reynolds Number
s	coordinate parallel to a curve
S	finite element assembly operator; boundary layer energy parameter
Sc	Schmidt Number
t	time
T	temperature
u	velocity vector
U	reference velocity
v	perturbation velocity vector; normal velocity
x_i	Cartesian coordinate system
x,y,z	rectangular coordinate system
Y	species mass fraction
β	pressure gradient parameter
γ	ratio of specific heats
∂R	closure of elliptic solution domain
δ	boundary layer thickness; Kronecker delta

Δ	increment
ϵ	kinematic turbulent viscosity; amplitude; belongs to
κ	coefficient
λ	multiplier; turbulence sublayer constant; period
μ	molecular viscosity
ρ	density
σ	integral kernel
τ	stress tensor; integral kernel
ϕ	perturbation potential function
Φ	scalar potential function; finite element functional
χ	domain of initial-value operator
ψ	x_3 scalar component of vector potential
Ψ	vector potential function
ω	x_3 scalar component of vorticity; Van Driest coefficient
Ω	vorticity vector; global solution domain
$\{\}$	column matrix
$[]$	square matrix
$\cup$	union
$\cap$	intersection

Superscripts		Subscripts	
T	matrix transpose	e	local reference condition
α	species identification	i,j,k,ℓ	tensor indices
$\hat{}$	unit vector	ℓ	evaluated on lower surface
$\rightarrow$	vector	m	m^{th} finite element subdomain
*	approximate solution	o	initial condition
-	constrained to closure	p	pressure coefficient
$\perp$	component normal to curve	t	partial derivative by time
//	component parallel to curve	u	evaluated on upper surface
		w	evaluated at the wall
		∞	global reference condition

THE FIELD EQUATIONS FOR AERODYNAMIC FLOW

The complete description of a state point in multi-dimensional aerodynamics is contained within the solution of a system of coupled, nonlinear, second order partial differential equations describing the conservation of mass, linear (or angular) momentum, and energy. To establish unique solutions, closure of the system is required by specification of appropriate constitutive behavior and boundary conditions. In conventional vector notation, and then repeated in the preferred Cartesian tensor notation (where the subscript comma implies the gradient operator, subscript comma t is the time partial derivative, and the subscript semicolon implies the generalized divergence operator, see ref. 15), the conservation form of the differential equation system is

$$\frac{\partial \rho}{\partial t} = -\nabla \cdot [\rho \vec{u}] \tag{1A}$$

$$\frac{\partial}{\partial t}(\rho \vec{u}) = -\nabla \cdot [\rho \vec{u}\vec{u} - \overleftrightarrow{\tau}] + \rho \vec{B} \tag{2A}$$

$$\frac{\partial}{\partial t}[\rho H - p] = -\nabla \cdot [\rho \vec{u} H - \overleftrightarrow{\tau} \cdot \vec{u} - k \nabla T] + \rho \dot{Q} \tag{3A}$$

$$\frac{\partial}{\partial t}(\rho Y^{\alpha}) = -\nabla \cdot [\rho \vec{u} Y^{\alpha} - \rho D \nabla Y^{\alpha}] \tag{4A}$$

$$\rho_{,t} = -[\rho u_i]_{;i} \tag{1}$$

$$(\rho u_i)_{,t} = -[\rho u_i u_j + p\delta_{ij} - \tau_{ij}]_{;j} + \rho B_i \tag{2}$$

$$(\rho H - p)_{,t} = -[\rho u_i H - \tau_{ij} u_j - k T_{,i}]_{;i} + \rho \dot{Q} \tag{3}$$

$$(\rho Y^{\alpha})_{,t} = -[\rho u_i Y^{\alpha} - \rho D Y^{\alpha}{}_{,i}]_{;i} \tag{4}$$

The dependent variables in eqn.(1)-(4) have their usual interpretation in fluid mechanics. The mass flow vector is ρu_i where ρ is the mass density

and u_i is the local velocity vector. In eqn.(2), B_i is an appropriate body force, and τ_{ij} is the diffusive (viscous) stress tensor. Eqn.(3) is written on stagnation enthalpy, H,p is the static pressure, T is the static temperature, and Q is the local heat generation rate. For multiple species flows, as might occur for example in powered lift configurations, Y^{α} is the mass fraction of the α^{th} species in eqn.(4), and D is the binary diffusion coefficient. Eqn.(4) also provides the means for tracing the transport of distinct flow field components.

As stated, the solution of eqn.(1)-(4) requires specification of constitutive relationships between the dependent variables and the diffusion coefficient D , the stress tensor τ_{ij}, and the effective viscosity and thermal conductivity. For compressible flows, an equation of state relating the thermodynamic variables is also required. Since predictions in both laminar and turbulent flows are required, and since the time-averaged form of eqn.(1)-(4) appears identical to those presented, by appropriate interpretation of the stress tensor, the general form of closure can be written as

$$\tau_{ij} = [\mu(T) + \rho\varepsilon_{ij}]f(u_{i;j} + u_{j;i}) \tag{5}$$

In eqn.(5), μ identifies the laminar molecular viscosity which is temperature dependent, and ε_{ij} is the effective transport tensor due to turbulence. As indicated, the diffusive stress tensor is assumed a functional of the symmetric velocity gradient (cf., Donaldson et al., ref. 18). For strictly laminer flow of a Newtonian fluid, eqn.(5) embodies Stokes' viscosity law

$$\tau_{ij} = 2\mu[E_{ij} - \frac{1}{3} E_{kk}\delta_{ij}] \tag{6}$$

which displays the linear functional dependence on the symmetric velocity gradient as

$$f(u_{i;j} + u_{j;i}) = E_{ij} \equiv \frac{1}{2} (u_{i;j} + u_{j;i}) \tag{7}$$

The thermodynamic properties are typically expressed as

$$p = p(\rho, Y^{\alpha}, T) \tag{8}$$

$$\begin{aligned} H &\equiv \sum_{\alpha} h^{\alpha} Y^{\alpha} + \frac{1}{2} u_i u_i \\ &= \sum_{\alpha} \int_{T_o}^{T} c_p^{\alpha} Y^{\alpha} dT + \frac{1}{2} u_i u_i \end{aligned} \tag{9}$$

$$D^{\alpha} = D(Y^{\alpha}, u_i) \tag{10}$$

Rather than attempting direct solution of eqn.(1)-(10), it is convenient to non-dimensionalize all variables to extract the useful non-dimensional groupings. Using standard procedures (ref. 15.), the non-dimensional form of eqn.(1)-(4) is

$$\rho_{,t} = -[\rho u_i]_{;i} \tag{11}$$

$$(\rho u_i)_{,t} = -\left[\rho u_i u_j + p\delta_{ij} - \frac{1}{Re}\tau_{ij}\right]_{;j} + \frac{1}{Fr}\rho b_i \tag{12}$$

$$\left(\rho H - (Ec)p\right)_{,t} = -\left[\rho u_i H - \frac{Ec}{Re}\tau_{ij} u_j - \frac{1}{Re\ Pr}\mu H_{,i}\right]_{;i} + \frac{1}{Re\ Pr_{\infty}}\rho\dot{Q} \tag{13}$$

$$(\rho Y^{\alpha})_{,t} = -\left[\rho u_i Y^{\alpha} - \frac{Le}{Pr}\mu Y^{\alpha}{}_{,i}\right]_{;i} \tag{14}$$

In eqn.(11)-(14), the important non-dimensional parameters for fluid mechanics are identified as

Reynolds Number: $$Re \equiv \frac{\rho_\infty U_\infty L}{\mu_\infty} \tag{15}$$

Prandtl Number: $$Pr \equiv \frac{c_p \mu}{k} \tag{16}$$

Eckert Number: $$Ec \equiv \frac{U_\infty^2}{c_{p_\infty} T_\infty} \tag{17}$$

Froude Number: $$Fr \equiv \frac{U_\infty^2}{Lg} \tag{18}$$

Lewis Number: $$Le \equiv \frac{\rho D}{\mu} Pr \tag{19}$$

It is also useful to define the Schmidt number from the above as

$$Sc \equiv \frac{Pr}{Le\ Re}$$

Note that, for a thermodynamically perfect fluid

$$Ec = (\gamma-1)M^2_\infty \tag{20}$$

where γ is the ratio of specific heats, and M_∞ is the reference Mach number defined as

$$M_\infty = \frac{U_\infty}{\sqrt{\gamma R T_\infty}} \tag{21}$$

where R is the universal gas constant divided by the molecular weight.

The solution of eqn.(11)-(14) is a formidable task, and there are several alternative forms and simplifications to the system that can render such solution more straightforward for non-trivial problem classes in aerodynamics. The Navier-Stokes equations primarily describe the behavior of the mass flow vector field, ρu_i. From vector field theory, we recognize that without loss of generality, we can describe ρu_i in terms of a scalar and a vector poten-

tial function, Φ and $\vec{\Psi}$ respectively, as

$$\rho\vec{u} = -\rho\,\vec{\nabla}\Phi + \vec{\nabla}\times\vec{\Psi} \tag{22A}$$

$$\rho u_i = -\rho\Phi_{,i} + e_{ijk}\,\Psi_{k,j} \tag{22}$$

The first equation employs conventional vector notation; the second illustrates the preferred indical form, and the decomposition in eqn.(22) is unique to within an arbitrary constant, provided $\vec{\Psi}$ satisfies the "gauge" condition, i.e., $\vec{\nabla}\cdot\vec{\Psi} = \Psi_{k;k} = 0$ (cf., ref. 19, App. I.). In terms common to fluid mechanics, Φ is called the (total) potential function, and $\vec{\Psi}$ is the three-dimensional equivalent of the familiar two-dimensional stream function.

Viewing eqn.(11), we observe that for steady or incompressible flows, the massflow vector field also satisfies the "gauge" condition, i.e., it is divergence-free. Inserting eqn.(22) into (11), and from the skew-symmetry properties of the Cartesian alternator, we obtain

$$(\rho u_i)_{;i} = (\rho\Phi_{,i})_{;i} = 0 \tag{23}$$

An elementary solution to eqn.(23) is that Φ vanishes everywhere. Hence, for all cases where eqn.(11) describes steady or incompressible flow, we may choose to analyze the flow using the transformation

$$\rho u_i = e_{ijk}\,\Psi_{k,j} \tag{24}$$

In this case, ρu_i is said to be a solenoidal vector field. An important additional aspect of this problem class is that the flow may be explicitly rotational. The vorticity $\vec{\Omega}$ is defined as the curl of velocity field; hence

$$\Omega_i \equiv e_{ijk}\,u_{k;j} \tag{25}$$

Substituting eqn.(24) into (25), utilizing the symmetry properties of alternator contractions, and noting that Ψ_k satisfies the gauge condition, the compatibility relation between stream function and vorticity is directly obtained as

$$\Omega_i = -\left[\frac{1}{\rho}\,\Psi_{i,j}\right]_{;j} + \Psi_{j;i}\left(\frac{1}{\rho}\right)_{,j} \tag{26}$$

Eqn.(26) may find considerable use in analysis of certain problem classes in aerodynamics.

We have an alternative choice for the aerodynamically important case of irrotational flow, wherein the curl of eqn.(22), or eqn.(25) vanishes identically by assumption. Again using the skew-symmetric properties of the alternator, and for Ψ_k satisfying the gauge condition, one obtains from eqn.(22)

$$e_{jik}\,(\rho u_i)_{,k} \equiv 0 = -\,\Psi_{k;jj} \tag{27}$$

If we set Ψ_k equal to zero everywhere, for irrotational flows we then have the identity,

$$\rho u_i = -\rho\Phi_{,i} \tag{28}$$

In this case, ρu_i is said to be a lamellar vector field.

We may elect to employ the primitive variable description for ρu_i, or may selectively employ the definitions in eqn.(24), (25) and/or (28). The particular choice depends upon the features of the differential equation system derived from eqn.(11)-(14) for each case of aerodynamic value.

Aerodynamic Potential Flow

The steady, isentropic flow of an inviscid, single-species perfect gas has been the focal point of research in aerodynamics for well over 70 years. A specific accounting of the simplifying assumptions is readily accomplished for the parent differential equation system, eqn.(11)-(14). Neglecting body forces, and discarding the species continuity equation as redundant, for this problem class we have

$$(\rho u_i)_{;i} = 0 \tag{29}$$

$$(\rho u_i\, u_j)_{;i} = -p_{,j} \tag{30}$$

$$c^2\, \rho_{,i} = p_{,i} \tag{31}$$

Since isentropic implies adiabatic and reversible, eqn.(13) is identically satisfied by H = constant . Eqn.(31), an alternative expression for this form of eqn.(13), defines the speed of sound in an isoenergetic perfect gas. Since the flow is assumed inviscid, the dispersive stress tensor, eqn.(5), vanishes identically. Eqn.(29)-(31) can be conveniently combined into a single differential equation on the velocity field, u_k . Substituting eqn.(31) plus the expansion of eqn.(29) into eqn.(30), one directly obtains the differential constraint for steady, inviscid isentropic flow as

$$\left[\delta_{ij} - \frac{u_i u_j}{c^2}\right] u_{i;j} = 0 \tag{32}$$

In eqn.(32), recall that c is the local speed of sound, conveniently defined in terms of a stagnation reference condition and the local velocity field by the isentropic energy equation in the form

$$c^2 = c_o^2 - \frac{\gamma-1}{2}\, u_k\, u_k \tag{33}$$

Eqn.(32) is a highly non-linear, first order partial differential equation written on the field behavior of the velocity vector u_k . It is valid for all Mach numbers, and as a function of local Mach number may selectively display elliptic, parabolic, and hyperbolic differential character. An important subclass corresponds to the additional constraint that the flow be irrotational. For this case, a useful restatement of eqn.(32) is obtained using eqn.(28). By direct substitution, the second order partial differential equation for determination of the distribution of the scalar potential function Φ is

$$\left[\delta_{ij} - \frac{\Phi_{,i}\,\Phi_{,j}}{c^2}\right] \Phi_{;ij} = 0 \qquad (34)$$

Eqn.(34) displays the mixed differential character as well. For $i = j$, the term in the bracket becomes of the form $[1 - M_{(i)}]$, where $M_{(i)}$ is the local Mach number of the flow in the coordinate direction $x_{(i)}$. Hence, for subsonic flows, eqn.(34) is elliptic, and from the theory of the solution of partial differential equations we require knowledge of an algebraic combination of Φ and its normal derivative, $\Phi_{,k}\hat{n}_k$ around the complete closure of the solution domain. For supersonic flows, one of the bracketed terms may become negative, and eqn.(34) then displays a mixed elliptic-hyperbolic character. In this instance, boundary specifications on Φ and/or its normal derivative are required on some non-characteristic curve. In the intermediate (transonic) speed range, eqn.(34) can exhibit a globally elliptic character within embedded hyperbolic and/or parabolic sub-domains, and the numerical solution procedure must recognize these distinct regions.

Regarding boundary conditions, we observe that specification of velocity on the closure of the solution domain will correspond to a gradient boundary condition specification on the scalar potential function, see eqn.(28). On an arbitrarily oriented closure segment, identified by a unit outward pointing normal vector, $\hat{n}_k$, eqn.(28) states that

$$\Phi_{,k}\,\hat{n}_k = -u_k\hat{n}_k \equiv -U^{\perp} \qquad (35)$$

where $U^{\perp}$ is the scalar component of velocity parallel to $\hat{n}_k$. As a special case, eqn.(35) states that the normal derivative of Φ must vanish on an impervious aerodynamic surface, since thereupon the local velocity vector must lie tangent to the surface.

The numerical solution of the general non-linear form of eqn.(34) is not commonly attempted. For specification of additional simplifying assumptions, which constrains the generality of the flow field description, alternative forms for eqn.(34) that are more tractable for numerical solutions using con-

ventional techniques can be obtained. By and large, the fundamental step is re-definition of the scalar potential function, eqn.(28), under the assumption of the preponderant existence of a preferred flow direction. Assuming this direction aligned with the x_1 coordinate axis, and identifying a reference velocity (U_∞) as parallel to this direction, re-define the local velocity field as

$$\rho u_i = \rho U_\infty \delta_{i1} + \rho v_i \tag{36}$$

Under the assumption that the perturbation velocity component, v_i, is small in magnitude in comparison to the freestream reference velocity, we can define a corresponding perturbation potential function as

$$\rho v_i = -\rho \phi_{,i} \tag{37}$$

Then, eqn.(28) takes the form

$$\rho u_i = -\rho \Phi_{,i} = \rho U_\infty \delta_{i1} - \rho \phi_{,i} \tag{38}$$

Substituting eqn.(38) into eqn.(32), and altering the reference condition in eqn.(33) to that corresponding to U_∞, and proceeding through the well known order of magnitude analysis (cf., ref. 20), for the subsonic and supersonic slender body approximation one obtains the linearized form of eqn.(34) written on either the total or perturbation potential function as

$$1 - M_\infty^2 \; \Phi_{;11} + \Phi_{;22} + \Phi_{;33} = 0 \tag{39}$$

The boundary conditions for solution of eqn.(39) are obtained from the definition in eqn.(38) in the manner analagous to the specification in eqn.(35). Eqn.(39) displays the mixed elliptic-parabolic-hyperbolic character of the full non-linear form, eqn.(34). For the final additional assumption of zero Mach number, or equivalently incompressible flow, eqn.(39) becomes the Laplacian on Φ, which is a linear elliptic-boundary value problem. It is this form whose numerical solution is typically computed for subsonic flows,

in combination with an independent variable transformation on the x_1 coordinate axis to account for a finite subsonic Mach number.

Flow fields of the subject problem class are also amenable to analysis using the definition of stream function, eqn.(24), provided the parent flow is either incompressible or steady. For the additional assumption of irrotational, eqn.(26) must vanish identically from the definition in eqn.(25); hence

$$\left[\frac{1}{\rho}\,\Psi_{k;i}\right]_{;i} - \left(\frac{1}{\rho}\right)_{,i}\,\Psi_{i;k} = 0 \tag{40}$$

Eqn.(40) states that the vector potential function, Ψ_k, satisfies a second-order linear partial differential equation of the Laplacian type provided that the stream function satisfies the gauge condition. Since, from its definition, density can never become negative, and since the first-order differential term in eqn.(40) does not affect overall characterization, eqn.(40) is uniformly elliptic and its solution requires knowledge of Ψ_k and/or the normal derivative, $\Psi_{k;j}\hat{n}_j$ on the complete closure of the solution domain. The vector potential function is simply a generalized concept of the two-dimensional stream function familiar to all. Therefore, Ψ_k equal to a constant implies existence of a stream hypersurface across which mass flow vanishes. Forming the outer product of the defining equation, eqn.(24), with an arbitrary unit vector $\hat{a}_\ell$ yields

$$\rho u_i \hat{a}_\ell = \varepsilon_{ijk}\,\Psi_{k,j}\,\hat{a}_\ell \tag{41}$$

For $\hat{a}_\ell$ parallel to the velocity vector u_i, the specified mass flux across a segment of the solution domain closure determines the distribution of Ψ_k on the corresponding surface. Conversely, for $\hat{a}_\ell$ lying parallel to the velocity vector u_i, eqn.(41) yields a normal gradient-type boundary condition constraint on stream function in terms of the parallel velocity component of the form

$$\frac{1}{\rho}\,\Psi_{k;j}\hat{n}_j = -U_k'' \tag{42}$$

It is instructive to contrast the form of the boundary condition constraints for the two potential functions, see eqn.(35) and (42). As a final simplification, in the instance of constant density flow, note that eqn.(40) degenerates to the linear Laplacian written on Ψ_k . In all instances, since both the scalar and vector potential functions are defined only to within an arbitrary constant, see eqn.(22), each function may be appropriately specified at some point on the solution domain closure for convenience.

Analysis of rotational, inviscid isentropic flow fields can be accomplished using either the scalar or vector potential function as well. Regarding the former, for linearized potential flow theory, the Kutta-Joukowski hypothesis states that the correct rotational flow pattern of any family of flows is the one flow with a finite velocity at the trailing edge of an airfoil. Hence, from the concept governing two-dimensional, irrotational incompressible flow about bodies resembling subsonic airfoils, one can complete an analysis of a family of flows for a given boundary and a given freestream velocity. These flows differ primarily in the amount of circulation; however, all but one will have an infinite velocity at the trailing edge. With use of Kutta condition, use of eqn.(34) or any of its simplifications is not contraindicated for rotational inviscid flows.

For rotational incompressible or steady flows, use of the vector potential function is straightforward. The derived compatibility eqn.(26) becomes in this instance

$$\left[\frac{1}{\rho}\cdot\Psi_{k,j}\right]_{;j} = -\Omega_k \tag{43}$$

Eqn.(43) states that the distribution of the stream function will be altered by the imbedded rotational character of the flow. Provided the flow is steady and inviscid, an analysis (discussed in the next section) shows that the rotational freestream will be "frozen" into the computed streamline distribution about an aerodynamic shape. Hence, by establishing an iterative procedure for solution of eqn.(43), one theoretically can determine the rotational flow about an arbitrarily shaped aerodynamic surface, with embedded freestream vorticity, using the vector potential function.

Aerodynamic Viscous Flow

The complete analytical characterization of an aerodynamic system requires an accounting for viscous effects. For conventional aerodynamic shapes at small angle of attack, these effects are essentially confined to the thin layer of fluid in direct contact with the aerodynamic surface. The remainder of the flow field is essentially free of viscosity effects and completely amenable to analysis using inviscid flow field concepts. These thin viscous layers are called boundary layer flows, and their analysis and understanding constitutes an extremely important branch in engineering and aerodynamics. Under a first-order of magnitude analysis (cf., Schlichting, ref. 21), for the steady boundary layer flow of a viscous compressible fluid described by the velocity vector

$$u_i = u_1\hat{\varepsilon}_1 + u_2\hat{\varepsilon}_2 + u_3\hat{\varepsilon}_3 \tag{44}$$

where the unit vector triad $\hat{\varepsilon}_i$ lies parallel to coordinate curves of a general Cartesian curvilinear coordinate system, the three-dimensional boundary layer equivalent of eqn.(11)-(14) takes the form

$$0 = (\rho u_i)_{;i} \tag{45}$$

$$\rho u_i u_{1;i} = \frac{1}{Re}\left[(\mu + \rho\varepsilon_{12})u_{1;2}\right]_{;2} - p_{,1} \tag{46}$$

$$0 = -p_{,2} \tag{47}$$

$$\rho u_i u_{3;i} = \frac{1}{Re}\left[(\mu + \rho\varepsilon_{12})u_{3;2}\right]_{;2} - p_{,3} \tag{48}$$

$$\rho u_i H_{,i} = \frac{1}{RePr}\left[\left(\mu + \rho\varepsilon_{12}\right) H_{,2}\right]_{;2} + \frac{Ec}{Re}\left(u_{1;2} + u_{3;2}\right)^2 \tag{49}$$

$$\rho u_i Y^{\alpha}_{,i} = \frac{Le}{Pr}\left[\left(\mu + \rho\varepsilon_{12}\right) Y^{\alpha}_{,2}\right]_{;2} \tag{50}$$

In the form presented, the use of a body-oriented orthogonal coordinate system attached to the aerodynamic surface is assumed, where x_1 is parallel to the predominate direction of flow and x_2 is assumed to lie everywhere perpendicular to the aerodynamic surface. For aerodynamic surfaces with local curvature distributions, the generalized semicolon subscript (;) differential notation will yield additional terms stemming from use of a curvilinear coordinate system in equations (45)-(50). Note that the flow may be laminar, transitional or turbulent.

Perhaps the most significant feature of the boundary layer equations, and their solution, is contained in eqn.(47). Under the first-order of magnitude simplifications, the transverse momentum equation yields the significant fact that the pressure distribution is constant throughout the bounday layer thickness. Hence, in the remaining momentum eqn.(46) and (48), pressure appears as a parameter only, being obtained from the inviscid flow field solution. Therefore, eqn.(46) and (48) are solved respectively as initial value problems for u_1 and u_3 with the pressure replaced by p_e, while eqn.(45) is recast into an initial-value problem for the x_2 distribution of the velocity component normal to the surface, u_2. For non-isoenergetic flows, eqn.(50) is also solved as an initial value problem for the distribution of stagnation enthalpy, H. It should be noted that the conventional two-dimensional boundary layer equations are a sub-set of the presented form, obtained by deleting eqn.(48) and excluding 3 as an admissible index for summation in eqn.(45)-(50). Finally, for single species flow, eqn.(50) may be deleted completely.

The initial and boundary conditions appropriate for solution of eqn.(45)-(50) are obtained in a straightforward manner, as all except (45) represent a general initial-valued, two-point elliptic boundary value problem in mathematics. On the aerodynamic surface, the no-slip boundary condition for the tangential velocity field yields

$$u_1(x_1,0,x_3) = u_3(x_1,0,x_3) = 0 \tag{51}$$

To account for suction or blowing at the aerodynamic surface, the corresponding constraint for solution of eqn.(45) becomes

$$u_2(x_1,0,x_3) \equiv v(x_1,x_3) \tag{52}$$

where v is the specified distribution of normal velocity. Similarly, at the freestream juncture ($x_2 = \delta$) between the boundary layer and potential flow, we require the boundary layer velocity distribution to be equal to that of the external inviscid flow, denoted by a subscript e, as

$$u_i(x_1,\delta,x_3) = u_{e_i}(x_1, x_3) \tag{53}$$

Typically, solution of eqn.(50) at the surface involves a convection-type boundary condition written in terms of the local static temperature as

$$-kT_{,i}\hat{n}_i = h[T - T_r] \tag{54}$$

At the freestream, the normal gradient of H typically vanishes as

$$H(x_1,\delta,x_3)_{,i}\,\hat{n}_i = 0 \tag{55}$$

Finally, the form of eqn.(55) is typically appropriate at $x_2 = 0$ and $x_2 = \delta$ for solution of eqn.(51), with H replaced by Y^α.

Since eqn.(46), (48)-(51) are also initial value problems in the x_1 coordinate direction, an initial profile distribution for each appropriate dependent variable is required. Denoting q as a generalized dependent variable, the solution of the equation system is initialized by specification of the form

$$q(0,x_2,x_3) \equiv q_0(x_2,x_3) \tag{56}$$

The presented two- and three-dimensional boundary layer equations are the most tractible form of the parent Navier-Stokes equations for numerical solution. Consequently, their range of applicability is considerably limited by geometric or flow field considerations. For merging viscous flows near trailing edges, or flap and slat combinations, or for powered lift configurations with their associated thick viscous non-isoenergetic flow fields, a more comprehensive form of differential equation description is required. For steady three-dimensional flows of this type, in bounded or open domains and meeting

certain requirements, a significant simplification can be made to the parent Navier-Stokes equations that renders three-dimensional solutions considerably more retractable with present computer hardware. This approximation, now known as the "parabolic Navier-Stokes equations," describes steady three-dimensional flows wherein: 1) a predominant flow direction is uniformly present, 2) in this direction (only) diffusion processes are negligible compared with convection, and 3) no disturbances are propogated upstream anti-parallel to this direction. For the velocity vector identified in eqn.(44), and for the same coordinate description of the solution space, the three-dimensional parabolic Navier-Stokes equations are of the form

$$0 = (\rho u_i)_{;i} \tag{57}$$

$$\rho u_j u_{i;j} = \frac{\left(1 - \delta_{\underline{kl}}\right)}{Re} \left[\left(\mu + \rho\varepsilon_{\underline{ik}}\right) U_{i;k}\right]_{;k} - p_{,i} \tag{58}$$

$$\rho u_i H_{,i} = \frac{\left(1 - \delta_{\underline{kl}}\right)}{Re} \left\{ \left[\frac{\left(\mu + \rho\varepsilon_{\underline{ik}}\right)}{Pr} H_{,k} \right]_{;k} - \left[\frac{1 - Pr}{Pr} \frac{\left(\mu + \rho\varepsilon_{\underline{ik}}\right)}{2} (u_j u_j)_{;k} \right]_{;k} \right.$$

$$\left. - \left[\frac{Sc - Pr}{ScPr} \left(\mu + \rho\varepsilon_{\underline{ik}}\right) \sum_{\alpha} h^{\alpha} Y^{\alpha}_{,k} \right]_{;k} \right\} \tag{59}$$

$$\rho u_i Y^{\alpha}_{,i} = \frac{\left(1 - \delta_{\underline{kl}}\right)}{Re} \left[\frac{\left(\mu + \rho\varepsilon_{\underline{ik}}\right)}{Sc} Y^{\alpha}_{,k} \right]_{;k} \tag{60}$$

The dominant differences between the parabolic Navier-Stokes equation system, (57)-(60), and the three-dimensional boundary layer eqn.(45)-(50), relate to dimensionality of the boundary value character and to the appearance of pressure. For boundary layer flow, eqn.(47) yielded a uniform pressure distribution imposed through the thickness of the boundary layer. In the parabolic Navier-Stokes system, pressure appears as a dependent variable and

its solution is required. The several forms of the pressure algorithm, to be discussed, depend upon the particular geometrical configuration under study. The other significant feature of the parabolic Navier-Stokes system is that the diffusion term (first right side term modified by $(1-\delta_{k\bar{1}})/Re$) is two-dimensional, spanning the plane whose normal is parallel to the direction of predominant flow. (The subscript bar notation indicates no summation; for k=1 only, $(1-\delta_{k\bar{1}})$ vanishes.) Hence, boundary condition statements on the three components of velocity as well as enthalpy and mass fraction must be specified everywhere on the closure of this two-dimensional plane. Identifying q for a generalized dependent variable, most physically realistic boundary condition constraints are of the form

$$a^{(1)}(x_i)q + a^{(2)}(x_i)q_{,k}\hat{n}_k = a^{(3)}(x_i) \tag{61}$$

In eqn.(61), the $a^{(i)}$ are user-specified coefficients; note that the corresponding boundary layer equation statements, eqn.(51)-(55), are all special cases of eqn.(61). As before, since the parabolic Navier-Stokes equation system contains an initial value description for each dependent variable, specification of the form of eqn.(56) is required for each dependent variable.

Dependent upon the geometry of the flow configuration, eqn.(57) and the three equations in (58) are selectively altered to obtain solution of the three components of velocity and the pressure distribution. For boundary layer-type flows (termed boundary region flow), since eqn.(57)-(60) encompass eqn.(45)-(50) as a special subset, the assumption of vanishing normal distribution of pressure may be valid. Hence, the inviscid pressure distribution is imposed upon the flow field. Pressure is again decoupled from the solution, the second of eqn.(58) is discarded, and eqn.(57) is employed to solve for the x_2 distribution of the corresponding velocity component u_2. For solution domains totally bounded by solid walls, as might occur in inlets or exhaust ducts for example, the theory of Patankar and Spalding (ref. 22) can be used to achieve a pressure solution. Their theoretical procedure involves a splitting of the pressure field computation by decomposition of the local static pressure into the form

$$p(x_i) = \bar{p}(x_1) + p'(x_2,x_3) \tag{62}$$

Determination of the x_1 component, $\bar{p}$, is obtained by integrating eqn.(57) over the cross-sectional area of the duct and accounting for the influences of wall shear (τ_w), area change ($A(x_1)$), and heat or mass addition to yield the solution form

$$\frac{d\bar{p}}{dx_1} = f\left(\rho u_1,\ A(x_1),\ \tau_w,\ Y^\alpha,\ T\right) \tag{63}$$

Note that eqn.(63) is an ordinary differential equation; its solution determines the (assumed uniform) axial pressure gradient appropriate for solution of the first of eqn.(58). To obtain solution for the distribution, in the transverse plane $p'(x_2,x_3)$, the divergence of the second two equations of (58) is taken and coupled with eqn.(57) to yield the solution form

$$(1 - \delta_{\underline{k}1})p'_{;kk} = f(\rho u_i,\ Y^\alpha,\ T) \tag{64}$$

As written, eqn.(64) is a two-dimensional elliptic boundary value problem of the Poisson type; the right side is a specified function of its arguments.

The previous approach is inappropriate for flows in completely unbounded domains. In this instance and coupled with an equation of state, eqn.(57) can be cast as a pure initial value problem on the three-dimensional pressure distribution, $p(x_i)$. In this case, eqn.(57) takes the form

$$\frac{dp(x_i)}{dx_1} = \frac{-RT}{u_1}\left[\rho u_{1;1} + (1 - \delta_{\underline{k}1})\,(\rho u_k)_{;k}\right] \tag{65}$$

where we have assumed valid the perfect gas law. Note that eqn.(65) is totally inappropriate for confined flows, since the right side becomes infinite at a wall where u_1 vanishes. For three-dimensional flows bounded by an aerodynamic surface and an inviscid freestream, the second of eqn.(58) yields an appropriate specific form for determination of transverse pressure distri-

bution as

$$\frac{dp(x_2)}{dx_2} = f(\rho u_i,\ T,\ p_e) \tag{66}$$

For the alternative case of a viscous flow field imbedded between two potential flows, as might occur in the trailing edge region downstream of an airfoil for example, a recasting of eqn.(57) into the form of eqn.(64) using the concepts of eq.(62) may be required. In all instances, the computation of pressure typically involves application of initial-value techniques coupled with the explicit assumption that pressure variation is a local phenomenon unaffected by downstream influences. For flow fields where this assumption is violated, use of the parabolic Navier-Stokes equation systems is probably contraindicated.

Solution of the boundary layer or parabolic forms of the Navier-Stokes equations is appropriate for flow fields where curvature effects are sufficiently modest such that streamwise separation does not occur. However, at larger angles of attack for an airfoil for example, the created adverse pressure gradient will retard the parent unidirectional-type flow to the point where the streamwise momentum is insufficient to keep the flow attached to the airfoil. The phenomenon of separation occurs, whereby the remaining unidirectional aerodynamic flow is separated from the aerodynamic surface by a suitably sized region of highly rotational viscous flow. For fully three-dimensional geometric configurations, characterization of these flows requires solution of the full Navier-Stokes eqn.(11)-(14). However, since solution of this form is typically not tractable on current generation computers, full Navier-Stokes solutions are generally limited to two-dimensional configurations.

The form presented as eqn.(11)-(14) can be used for solution of two-dimensional viscous flows. However, for steady or incompressible cases, an alternative formulation can be completed that takes advantage of the vector field character of eqn.(11). For this case, eqn.(24) takes the specific form

$$\begin{aligned} \rho u_i &= e_{3ij}\ \Psi_{3,j} \\ &\equiv e_{3ij}\ \psi_{,j} \end{aligned} \tag{67}$$

It is significant to note that only the x_3 scalar component of the vector potential function is required to characterize two-dimensional flows. Similarly, eqn.(25) becomes

$$\Omega_3 \equiv \omega = e_{3ij}\, u_{j,i} \tag{68}$$

The compatibility equation, eqn.(26), becomes for two-dimensional flow, using eqn.(67) and (68)

$$0 = \left[\frac{1}{\rho}\ \psi_{,j}\right]_{;j} + \omega \tag{69}$$

In terms of stream function and vorticity, the momentum equation (12), of the Navier-Stokes system for two-dimensional steady or incompressible flows, becomes considerably simplified (ref. 15) to the form of the vorticity transport equation.

$$\rho\omega_{,t} = \frac{1}{Re}\ \left[\mu\omega_{,j} - \mu_{,j}\omega - \mu_{,k}\ \left(2\psi_{,k}\right)_{;j}\right]_{;j}$$

$$- e_{3ki}\left[(\omega\psi_{,i})_{;k} - \frac{1}{2}\,(\psi_{,\ell})^2_{;i}\ \ \left(\frac{1}{\rho}\right)_{,k}\right] \tag{70}$$

The most significant feature of eqn.(70) is the disappearance of pressure as a coupled dynamic variable. Hence, eqn.(69) and (70) constitute a closed system for determination of two-dimensional rotational viscous aerodynamic flows. The stagnation enthalpy and species continuity equations, eqn.(13)-(14), remain as presented except for substitution of eqn.(67) for the terms involving velocity.

As stated before, eqn.(69) is an elliptic boundary value problem since density never vanishes and is always positive. Therefore, for boundary conditions we require knowledge of ψ and/or its normal derivative everywhere on the closure of the solution domain. For finite Reynolds number, eqn.(70) is also an elliptic boundary value problem coupled with initial-value behavior due to the time derivative (for incompressible flows only). Hence, we also require knowledge of ω or its normal derivative everywhere on the closure

of the solution domain. Since the defining eqn.(68) is valid throughout the solution domain as well as its closure, boundary condition specifications on vorticity are obtained from eqn.(68) and (69). The numerically consequential vorticity boundary condition becomes the imposition of the no-slip wall; the equivalent embodiment in vorticity is

$$\omega = - \frac{d^2\psi}{dn^2} \tag{71}$$

In eqn.(71), n is the coordinate normal to the local closure segment of the solution domain. To evaluate eqn.(71), it is necessary to form the second derivative of the streamfunction distribution on the closure. Several forms have been determined as appropriate, see Roache (ref. 23, Section III.C).

The pressure distribution may be recovered from the vorticity-stream function characterization of a Navier-Stokes solution by evaluating the momentum equation, eqn.(12). Two alternatives exist; eqn.(12) can be differentiated by the divergence operator yielding a boundary-value specification on pressure involving the Laplacian operator. However, since we are primarily interested in pressure distributions on aerodynamic surfaces, an alternative formulation exists which can be of value. Form the vector contraction of eqn.(12) with an infinitisimal displacement vector dx_i and integrate over any curve; this yields

$$\int p_{,j}\delta_{ij}dx_i = -\int \left[\rho u_i u_j - \frac{1}{Re}\ \tau_{ij}\right]_{;j} dx_i - \frac{\partial}{\partial t}\int \rho u_i dx_i \tag{72}$$

Note that the left side of eqn.(72) is the integral of a perfect differential and thus independent of path. Hence, the pressure at any point in the field can be determined, in comparison to some reference value, by integration over an arbitrary (the easiest) path between the two points. Denoting the integrals of perfect differentials by Δ, completing the indicated integrals, and performing numerous integration by parts, the final form for eqn.(72) becomes

$$\Delta p = \Delta \left\{ \frac{\varepsilon_{3jk}}{Re} \left[\left(\left(\frac{\mu}{\rho} + \varepsilon \right) \psi_{,k} \right)_{;j} - \frac{2(\mu + \rho\varepsilon)}{3} \psi_{,k} \left(\frac{1}{\rho} \right)_{,j} \right] - \frac{1}{\rho} (\psi_{,k})^2 \right\}$$

$$+ \frac{\varepsilon_{3ik}}{Re} \int \left\{ \left(\left(\frac{\mu}{\rho} + \varepsilon \right) \psi_{,k} \right)_{;j} - (\mu + \rho\varepsilon)_{,j} \frac{1}{\rho} \psi_{,k} \right\}_{;j} dx_i \qquad (73)$$

$$+ \int \left\{ \left(\frac{1}{\rho} \right) \psi_{,i} \psi_{,j} \right\}_{;j} dx_i$$

In eqn.(73), the first curly bracket contains terms which are point dependent, the result of integrating perfect differentials. The second and third brackets require integration, thus selection of path. While the appearance of eqn.(73) is formidable, its numerical evaluation utilizes well-known techniques.

As a final observation, we noted in our earlier discussions that for steady, constant-density inviscid rotational flows, the vorticity was frozen into the streamline distribution. This can be readily determined from eqn.(70), the vorticity transport equation. The complete first term vanishes identically for inviscid flow, while the left and last right side terms vanish identically for steady, constant density flows. Hence, the sole term remaining for this case is due to convection. In terms of a streamline coordinate, denoted as $s(x_i)$, eqn.(70) can be written in scalar notation in terms of the velocity as

$$u \frac{\partial \omega}{\partial s} = 0 \qquad (74)$$

Since the streamline speed u does not vanish, satisfaction of eqn.(74) is obtained only for vorticity ω vanishing identically or not varying in the streamline coordinate direction. Hence, the previous observation for aerodynamic potential flow is confirmed from the vorticity transport equation. It is useful to note that the form of eqn.(74) is quite identical to Bernoulli's law for determination of pressure distributions along inviscid streamlines.

$$u \frac{\partial \vec{u}}{\partial s} = - \frac{1}{\rho} \vec{\nabla} p \qquad (75)$$

Eqn.(75) is utilized for determination of surface pressure distributions using the velocity distribution computed from an inviscid flow field analysis.

FINITE ELEMENT SOLUTION ALGORITHM

Various forms of the Navier-Stokes equations have been developed as appropriate for analysis of distinct configurations in aerodynamic flow. For an inviscid irrotational analysis, eqn.(34) is the preferred parent form, written on scalar potential function, with eqn.(39) obtained following some linearizing assumptions. Vector streamfunction is applicable to rotational flows as well; its distribution is established via solution of eqn.(40) or (43) appropriately. Viscous flow analyses have fallen into several categories. For a completely attached viscous boundary layer between the aerodynamic surface and the freestream, solution of the two- or three-dimensional boundary layer eqn.(45)-(50) is appropriate. For merging viscous flows near trailing edges, or flap and slat combinations, or for powered lift configurations with thick viscous non-isoenergetic flow fields, the more comprehensive parabolic Navier-Stokes system is appropriate, eqn.(57)-(60), provided the flow remains unidirectional. Finally, analysis of omnidirectional viscous flows requires solution of the complete Navier-Stokes equations, either in the parent form of eqn.(11)-(14) or for two-dimensional configurations, eqn.(69)-(70). For the subsonic flows of present interest, each member of the derived differential equation systems (except for instances with specific retention of the continuity eqn.(11)) is uniformly cast as an elliptic boundary value problem of mathematical physics with individual instances of initial-value coupling. Specifically, identifying $q(x_i,\chi)$ as a generalized dependent variable of interest, each of the subject partial differential equations is a special case of the general, second-order non-linear partial differential equation

$$L(q) \equiv \kappa\left[K_{ij}(q)q_{,i}\right]_{;j} + f(q,q_{,i},x_i) - g(g,\chi) = 0 \qquad (76)$$

In eqn.(76), f and g are specified functions of their arguments, χ is identified with x_1 for boundary layer or parabolic flows or time for transient flows, and the x_i are the coordinates for which second-order derivatives exist in the lead term. For this term, κ is a scalar constant and $k_{ij}(q)$ is the generalized diffusion tensor, and both become uniquely specified by identification of q with each of the dependent variables associated with the particular equation system of interest. The finite element solution algorithm

is based upon the assumption that $L(q)$ is uniformly parabolic within a bounded open domain Ω ; that is, the lead term in eqn.(76) is uniformly elliptic within its domain R , with closure ∂R , where

$$\Omega = R \times (\chi_o, \chi) \tag{77}$$

and $\chi_o \leq \chi$. If eqn.(76) is uniformly parabolic, unique solutions for q are obtained upon specification of functional constraints on the closure of Ω, $\partial\Omega \equiv \partial R \times [\chi_o, \chi)$, and an initial-condition specification on $R \cup \partial R \times \chi_o$. For constraints on $\partial\Omega$, the general form relates the function and its normal derivative everywhere on the closure ∂R as

$$\ell(q) \equiv a^{(1)}\, q(\bar{x}_i, \chi) + a^{(2)}\, K_{ij}\, q(\bar{x}_i, \chi)_{,i}\, \hat{n}_j - a^{(3)} \equiv 0 \tag{78}$$

In eqn.(78), the $a^{(i)}\,(\bar{x}_i, \chi)$ are user-specified coefficients, the superscript bar notation constrains x_i to ∂R , and $\hat{n}_j$ is the local outward-pointing unit normal vector. For an initial distribution, assume that

$$q(x_i, \chi_o) \equiv q_o(x_i) \tag{79}$$

is given throughout $R \cup \partial R \times \chi_o$.

The finite element solution algorithm is established for the equation system (76)-(79) by using the method of weighted residuals (MWR) formulated on a local basis. Since eqn.(76) is valid throughout Ω , it is valid within disjoint interior subdomains Ω_m described by $(x_i, \chi) \in R_m \times [\chi_o, \chi)$, called finite elements, wherein $\cup R_m = R$. An approximate solution for q within $R_m \times [\chi_o, \chi)$, called $q_m^*(x_i, \chi)$, is formed by expansion into a series solution of the form

$$q_m^*\,(x_i, \chi) \equiv \left\{\Phi(x_i)\right\}^T \left\{Q(\chi)\right\}_m \tag{80}$$

In eqn.(80), the functionals $\Phi_k(x_i)$ are subsets of a function set that is complete on R_m. The expansion coefficients $Q_k(\chi)$ represent the unknown χ-dependent values of $q_m^*(x_i, \chi)$ at specific locations interior to R_m and on the closure ∂R_m, called nodes of the finite element discretization of R .

To establish the values taken by the expansion coefficients in eqn.(80), require that the local error in the approximate solution to both the differential equation $L(q_m^*)$ and the boundary condition statement $\ell(q_m^*)$ on for $\partial R_m \cap \partial R \neq 0$, be rendered orthogonal to the space of the approximation functions. By employing an algebraic multiplier λ, the resultant equation sets can be combined as

$$\underset{m}{S}\left[\int_{R_m} \left\{\Phi(x_i)\right\} L(q_m^*)\, d\tau - \lambda \int_{\partial R_m \cap \partial R} \left\{\Phi(x_i)\right\} \ell(q_m^*)\, d\sigma\right] \equiv \{0\} \quad (81)$$

where $\underset{m}{S}$ is the mapping function from the finite element subspace R_m to the global domain R, commonly termed the assembly operator. The number of eqn.(81) prior to assembly is identical with the number of node points of the finite element R_m.

Eqn.(81) forms the basic operation of the finite element solution algorithm and of the COMOC computer program to be described. The lead term can be rearranged, and λ determined by means of a Green-Gauss theorem:

$$\int_{R_m} \left\{\Phi(x_i)\right\} \kappa \left[K_{ij} q_m^*{}_{,i}\right]_{,j} d\tau = \kappa \oint_{\partial R_m} \left\{\Phi(x_i)\right\} K_{ij} q_m^*{}_{,i} \hat{n}_j\, d\sigma$$

$$- \kappa \int_{R_m} \left\{\Phi(x_i)\right\}_{,j} K_{ij} q_m^*{}_{,i}\, d\tau \quad (82)$$

For $\partial R \cap \partial R_m$ nonvanishing in eqn.(82), the corresponding segment of the closed-surface integral will cancel the boundary condition contribution (eqn.(81)) by identifying $\lambda a^{(2)}$ with κ of eqn.(76). The contributions to the closed-surface integral eqn.(82), where $\partial R_m \cap \partial R = 0$, can be made to vanish (ref. 15). When eqn.(78)-(82) are combined, the globally assembled finite-element solution algorithm for the representative partial differential equation system becomes

$$\underset{m}{S}\left[-\kappa\int_{R_m}\{\Phi\}_{,j}\;K_{ij}q^*_{m,i}\,d\tau+\int_{R_m}\{\Phi\}\,(f^*_m-g^*_m)\,d\tau\right.$$

$$\left.-\kappa\int_{\partial R_m\cap\partial R}\{\Phi\}\;\left(a^{(1)}_m q^*_m-a^{(3)}_m\right)\,d\sigma\right]=\{0\}\qquad(83)$$

The rank of the global equation system (83) is identical with the total number of node points on $R\ \partial R$ for which the dependent variable requires solution. Eqn.(83) is a first-order, ordinary differential system, and the matrix structure is sparse and banded. Solution of this system is obtained by COMOC using a predictor-corrector finite-difference numerical integration algorithm (ref. 14).

A solution algorithm is required for the continuity equation, which is retained as eqn.(45) or (57) for boundary-layer or parabolic flows. When retained, it describes an initial-value problem on ρu_2 or p as a function of x_2, with x_1 (χ) and x_3 appearing as parameters. The solution approximation function need span only the transverse coordinate direction as

$$q^*_m=\left\{\Phi(x_2)\right\}^T\left\{Q(x_1,x_3)\right\}_m\qquad(84)$$

The matrix elements of Q are nodal values of ρu^*_2 or p^*; their functional dependence requires solution of eqn.(45), (63), (66) or (65) along lines (x_1,x_3) or (x_2) equal a constant. Since each exists in standard form as an ordinary differential equation, direct numerical integration or quadrature yields the required solution at node points of the discretization.

COMOC COMPUTER PROGRAM

The COMOC computer program system is being developed to transmit the rapid theoretical progress in finite element solution methodology into a viable numerical solution capability. In the course of establishing this general-purpose concept, several Variants of COMOC have been developed for specific problem classes, including transient thermal and thermo-structural analysis, the two-dimensional transient Navier-Stokes equations, and the three-dimensional boundary-region, and parabolic Navier-Stokes equations. These initial forms have now been coalesced onto two advanced Variants. The Computational Continuum Mechanics Variant is operational on IBM 360/ and 370/ computers; it serves as a research test bed and can solve multidisciplinary problems characterized by a single differential equation description including transient and steady-state thermal analysis, thermo-elasto-statics, potential fluid flow, and magneto- and electro-statics. It contains automated data generation features using curved iso-parametric two-dimensional elements to model non-regular shaped solution domains, and input/output graphics to facilitate data management and solution interpretation. The Navier-Stokes Variant is operational on the IBM 360/ and CDC 6000 series computers; it solves the multiple-differential equation descriptions characteristic of viscous fluid mechanics including transient-incompressible, and steady-compressible, multiple-species complete two-dimensional Navier-Stokes equations, as well as the two- and three-dimensional compressible, reacting, multiple-species boundary layer, boundary region and confined-flow parabolic Navier-Stokes equations. It also contains output graphics and an automated data generator for regular-shaped solution domains. An on-line restart feature allows the user to switch between boundary-region and parabolic Navier-Stokes systems according to the requirements of the problem at hand.

The finite element solution algorithm is utilized, as we observed in the previous section, to cast the original initial-valued, or pure-elliptic boundary-value problem description into large-order systems with a purely initial-value or algebraic character. COMOC then integrates or equation solves the discretized equivalent of the governing equation system. Initial distributions of all dependent variables may be appropriately specified or computed, and boundary constraints for each dependent variable can be specified on

arbitrarily disjoint segments of the solution domain closure. The solutions for each dependent variable, and all computed parameters, are established at node points lying on a specifiably nonregular computational lattice, formed by plane triangulation of the elliptic portion of the solution domain. Each of the computational triangles is spanned by a linear approximation function used for all independent and dependent variables as well as all solution parameters.

The COMOC system is being built upon the macrostructure illustrated in fig. 1. The main executive routine allocates core by means of a variable dimensioning scheme based upon the total degrees of freedom of the global problem. The size of the largest problem that can be solved is thus limited only by the available core of the computer in use. The precise mix between dependent variables and parameters, and fineness of the discretization, is user-specifiable and widely variable. The input module serves its standard function for all arrays of dependent variables, parameters, and geometric coordinates. The discretization module forms the finite-element discretization of the elliptic solution domain and evaluates all required finite-element nonstandard matrices and standard-matrix multipliers. The initialization module computes the remaining initial parametric data required to start the solution. The integration module constitutes the primary execution sequence of problem solution, and primarily utilizes a highly stable, predictor-corrector integration algorithm for the column vector of unknowns of the solution. Calls to auxiliary routines for parameter evaluation (viscosity, Prandtl number, source terms, combustion parameters, etc.) as specified functions of dependent and/or independent variables, as well as calls for equation solving algebraic systems, are governed by the integration module. The output module is similarly addressed from the integration sequence and serves its standard function via a highly automated array display algorithm. Both Variants of COMOC can execute distinct problems in sequence, and contain automatic restart capability to continue solutions.

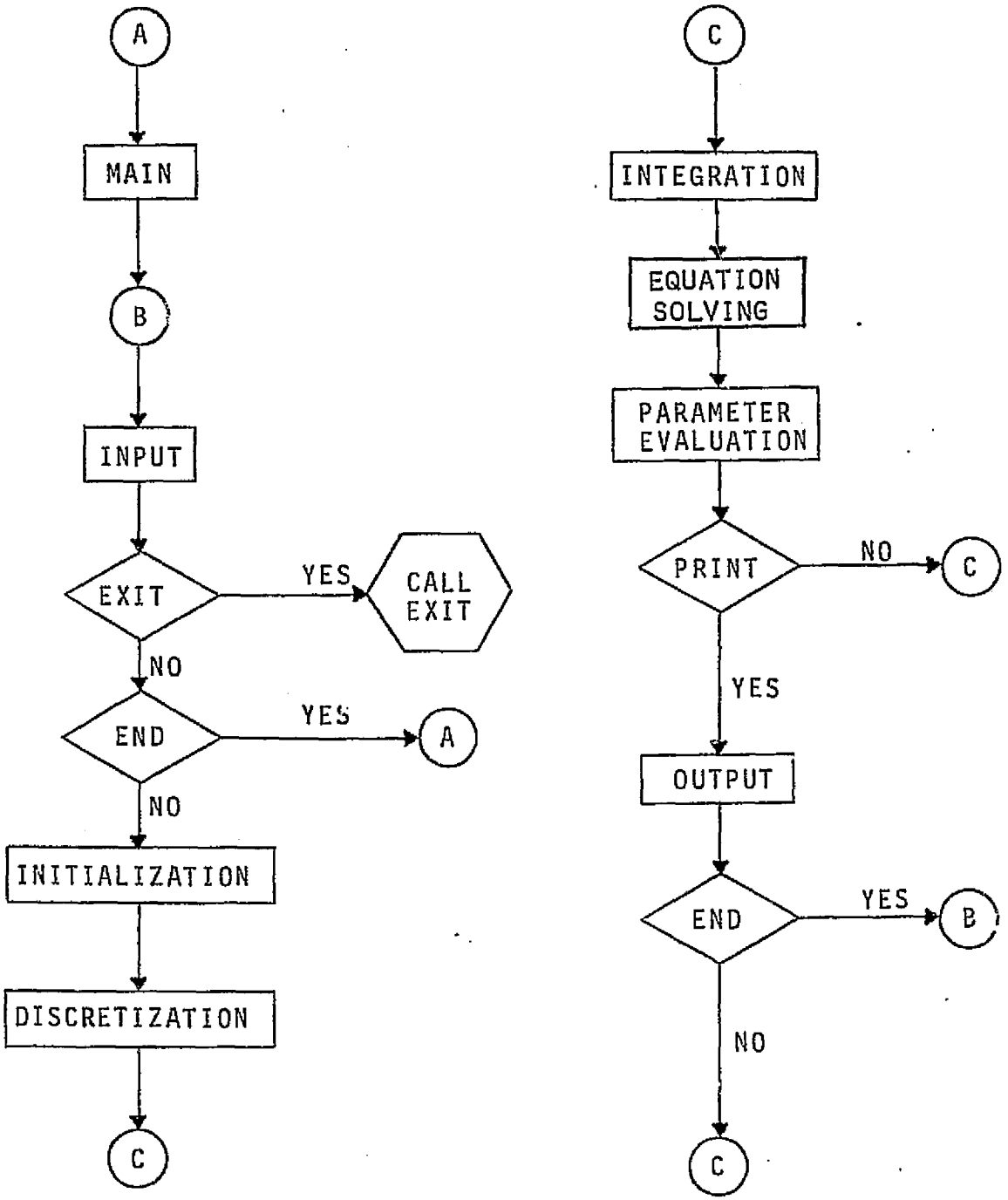

Figure 1. COMOC Macro-structure.

NUMERICAL SOLUTIONS IN AERODYNAMICS

Both operational Variants of the COMOC system have been exercised to obtain finite element characterization of various aerodynamic flow field configurations. Linearized and complete potential flow solutions have been generated by the Continuum Mechanics Variant, over curvilinear and airfoil configurations, to assess solution accuracy and to demonstrate features of finite element solutions. Viscous flow computations using the Navier-Stokes Variant include boundary layer prediction in a pressure gradient, parabolic Navier-Stokes solution of a trailing edge wake simulation, and a transient Navier-Stokes solution for decay of an aerodynamic shed vortex.

Aerodynamic Potential Flow Solutions

An informative problem geometry to evaluate finite element solution of linearized potential flow, eqn.(39), corresponds to subsonic, inviscid, isoenergetic flow over a wave-shaped wall, see fig. 2a. A linearized analytical solution can be obtained (cf. ref. 20, p. 458), for the ratio of wavelength (λ) to amplitude (ε) small, as

$$\Phi(x,y) = U_\infty \left[- x + \frac{\varepsilon}{\sqrt{1-M_\infty^2}} \cos\left(\frac{2\pi x}{\lambda}\right) \exp\left(-\frac{2\pi y}{\lambda}\sqrt{1-M_\infty^2}\right)\right] \tag{85}$$

for a sinusoidal wall described by

$$y_w(x) = \varepsilon \sin \frac{2\pi x}{\lambda} \tag{86}$$

assuming a uniform inflow of U_∞ at $x = 0$ and a freestream Mach number of M_∞. An absolute accuracy assessment is possible, and the essential geometrical character requires a specified gradient boundary condition on a non-coordinate surface. The key computational output is surface velocity distribution, since from Bernoulli's law, eqn.(75), the corresponding incompressible surface pressure distribution can be determined as

$$\begin{aligned} p(x,y_w) &= p_0 - \frac{1}{2}\rho_\infty u_k u_k \\ &= p_0 - \frac{1}{2}\rho_\infty \Phi_{,k} \Phi_{,k} \end{aligned} \tag{87}$$

The last form is obtained using eqn.(28); formation of the indicated vector inner product, from the discretized computational solution for Φ , is achieved using the finite element assembly operator $\underset{m}{S}$, see eqn.(81) and ref. 15.

The existence of various symmetry planes in the problem domain can be effectively utilized to reduce the number of finite elements required to generate a solution. Shown in fig. 2b-2c are economical domain closures and appropriate boundary condition specifications for a potential flow solution using either Φ or Ψ . For the sample problem,

$$U_\infty = 32 \text{ m/s}$$
$$M_\infty = 0.2$$
$$\varepsilon/\lambda = 0.025$$
$$\lambda = 2\pi$$

For the discrete approximation, the infinity boundary was chosen to lie at $y = 60\varepsilon$ to insure that application of the zero gradient boundary condition was valid. The computational grid, consisting of 240 triangular finite elements, was automatically generated from coordinate data describing vertex and mid-side nodal coordinates of two "super elements" as illustrated to the right in fig. 3a. A plot of the computed equipotential distribution appears in fig. 3b.

Since the potential equation is elliptic, boundary condition specification is required on all domain boundaries. Indication of adequate discretization, to allow determination of accurate slope boundary condition representation, is noted both at the wall and at the upper boundary. The numerical and analytical solutions are compared in table 1, and the location of the maximum error is noted. To evaluate surface pressure, eqn.(87), the computed potential function distribution is analytically differentiated using eqn.(80), and assembled over the entire domain to obtain scalar velocities and pressure along the wall. It is interesting to note that the level of velocity error is equal to that of the error in potential function, even though the former requires differentiation. The largest velocity error is 2.3%, indicating good accuracy for the coarse finite element mesh used. Since the pressure coefficient is related to the square of velocity, the corresponding maximum error in surface pressure is 5.3%.

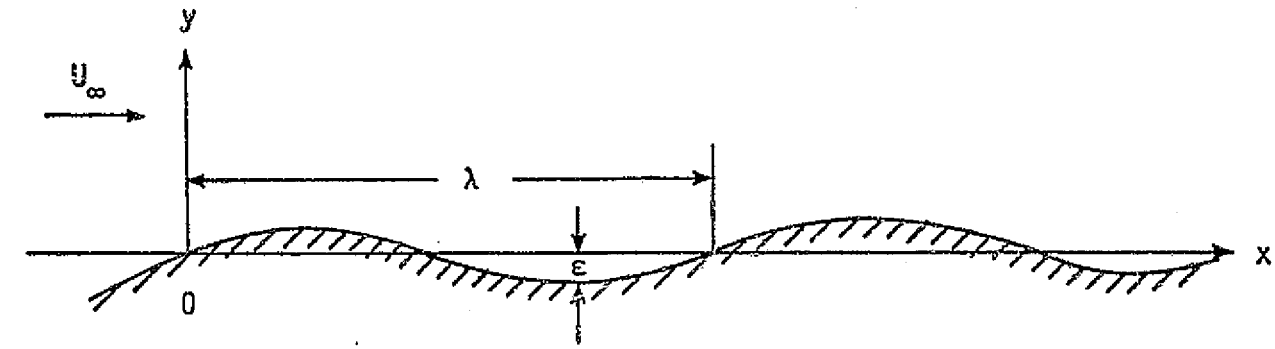

a) Geometry

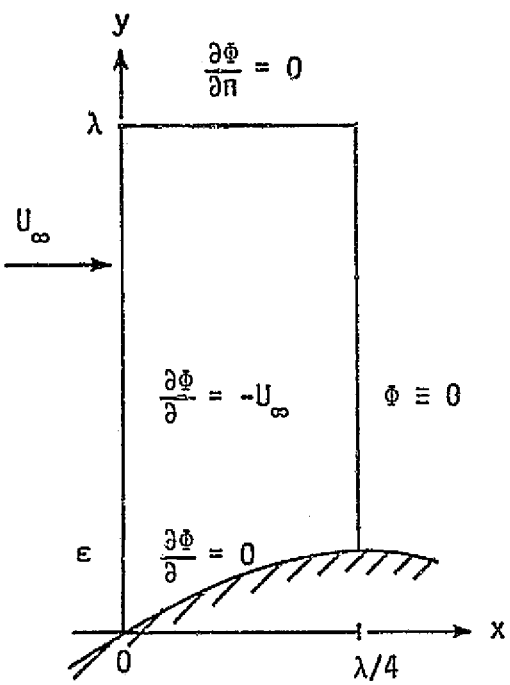

b) Solution domain for scalar potential

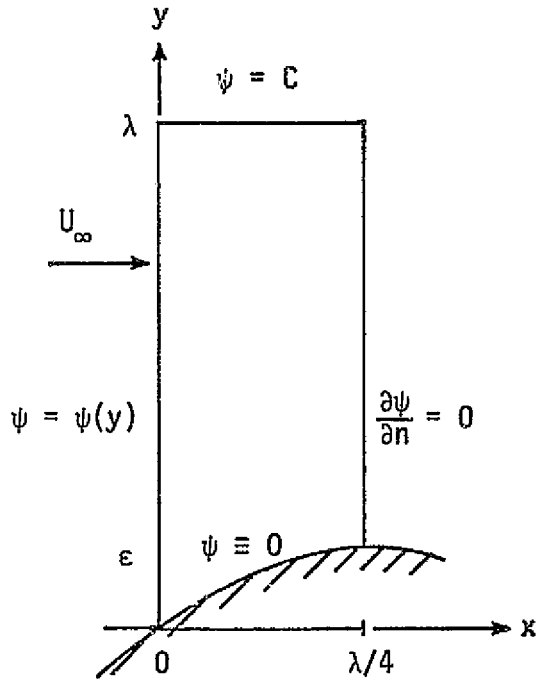

c) Solution domain for vector potential

Figure 2. Flow Over a Wave-Shaped Wall

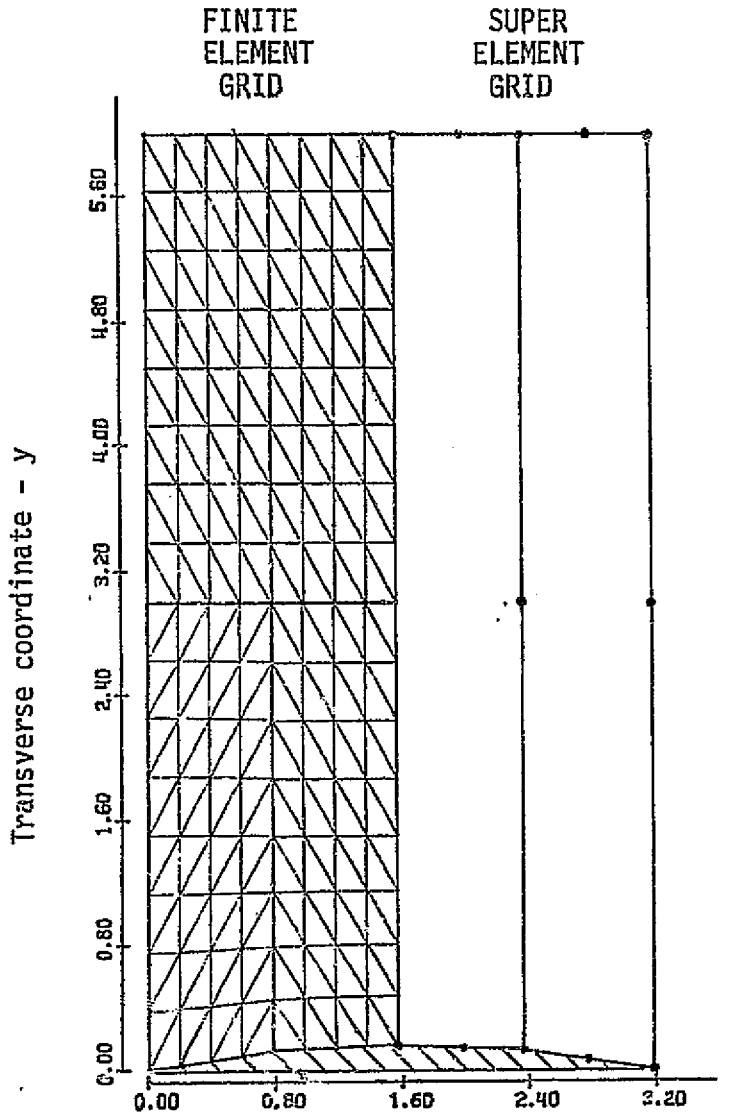

a) Discretization

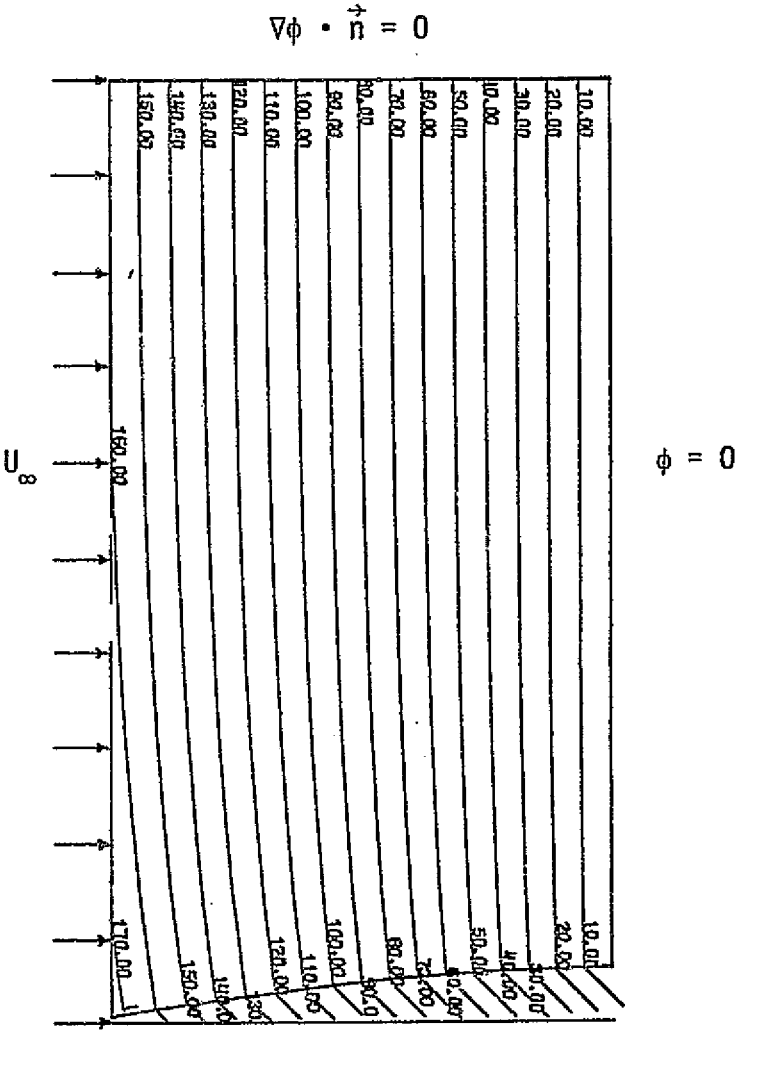

b) Equipotential distribution

Figure 3. Wave-Shaped Wall Solution Domain Discretization and Computed Equipotential Distribution.

Table 1. Potential Flow Over a Wave-Shaped Wall

Potential Function - Φ			Surface Velocity - $\sqrt{u_k\, u_k}$		
Analytical	COMOC	Error, %	Analytical	COMOC	Error, %
166.2	166.7	.3	97.18	97.15	.03
153.2	153.8	.4	99.05	98.16	.91
140.0	140.7	.5	100.80	99.54	1.25
126.5	127.4	.7	102.40	100.85	1.51
112.9	113.9	.9	103.83	102.12	1.70
99.1	100.2	1.0	105.10	104.33	.74
85.2	86.4	1.0	106.19	104.34	1.75
71.1	72.3	1.7	107.11	106.76	.33
57.0	58.1	1.9	107.86	108.16	.28
42.8	43.7	2.1*	108.45	109.42	.90
28.6	29.2	2.1*	108.86	110.54	1.50
14.3	14.6	2.1*	109.11	111.62	2.30*
0.	0.	0.	109.20	110.55	1.20

*Maximum Local Error

From the proven convergence character of the finite element solutions of linear (ref. 3) and non-linear (ref. 14,15) field problems, the 5% error in pressure could be reduced to about 1% by a uniform doubling of the fineness of the employed discretization. Unfortunately, the computer CPU required to obtain the more accurate solution also increases dramatically (by a factor of up to 8). Bearing this in mind, computational experiments were conducted to ascertain the influence of particular selected discretizations and closure locations (especially the infinity boundaries) on solution accuracy. For this study, however, the full tensor potential flow equation was solved, eqn.(34), using a linear iteration algorithm and sequential update of the effective diffusion tensor, $[\delta_{ij} - c^{-2}\, \Phi_{,i}\, \Phi_{,j}]$. The geometry selected is a symmetric NACA 0015 airfoil at zero angle of attack in subsonic flow in an inviscid wind tunnel, see fig. 4.

Since the circulation is zero for this case, only half the airfoil geometry need be considered, and the Kutta condition is intrinsic. The flow domain was automatically discretized by COMOC into 192 triangular finite elements, from user specification of the nodal coordinates of a coarse discretization consisting of three super elements, fig. 4 . The infinite boundary (tunnel wall) was set at about 13 airfoil thicknesses from the centerline.

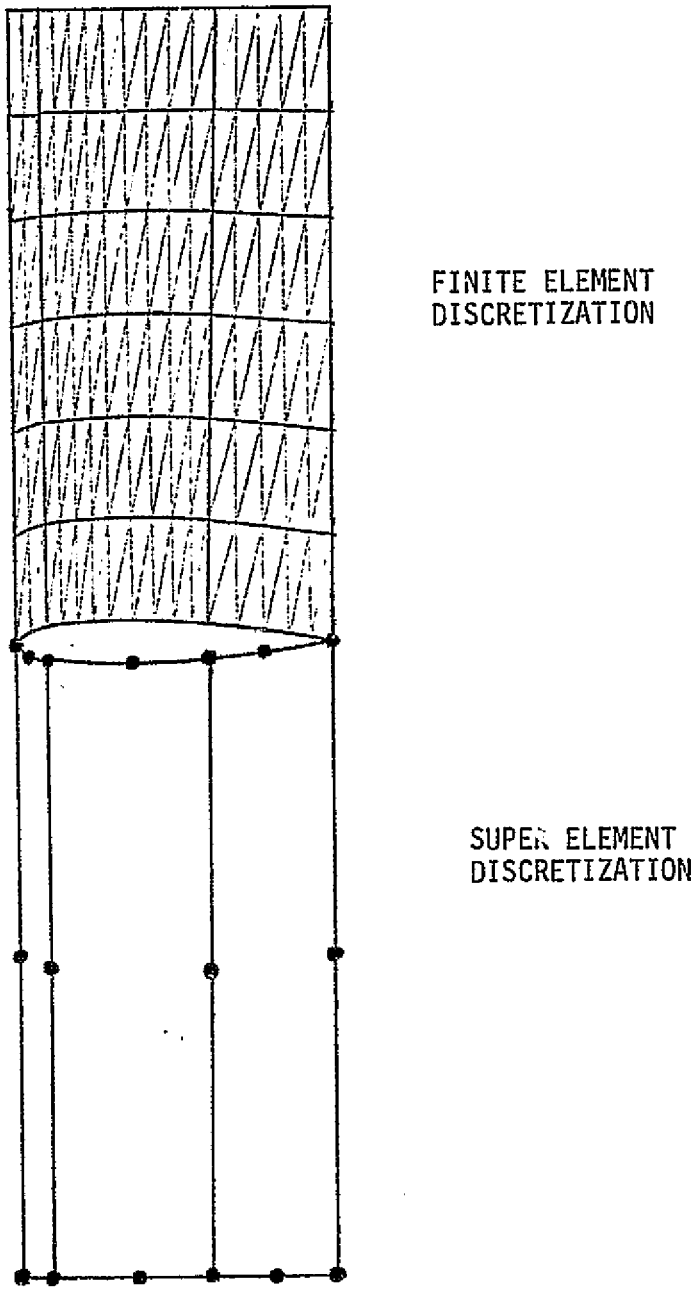

Figure 4. Finite Element Discretization for NACA 0015 Airfoil.

Flow conditions correspond to air at $M_\infty = 0.1$ and uniform velocity at the airfoil leading edge. Figure 5 presents the resultant computed pressure distribution (C_p) obtained from eqn. (87), along the airfoil surface compared with a conformal transformation solution (ref. 24, p. 324). While the solution trends are consistent, the "peaky" finite element results indicate the selected discretization was inadequate for definition of the large velocity gradients occurring at the airfoil leading edge. This problem existed but was less apparent in the wavy-wall solution, due to the much lower leading edge curvature, see fig. 6. Even though both finite element solutions used approximately identical discretization fineness, redefinition and refinement is required for the airfoil leading edge.

Several numerical experiments were conducted to evaluate discretization influences on solution accuracy. Equation (34) defines an elliptic boundary value problem in subsonic flow; it therefore is inappropriate to have either the airfoil leading or trailing edge coincide with the solution domain closure, even though the finite element algorithm solves for boundary nodes lying on symmetry planes (gradient boundary condition) along with interior nodes, see eqn.(83). While retaining the discretization fineness of fig. 4, additional regions extending one chord length upstream and downstream of the airfoil were added to the solution domain. The computational discretization, containing approximately 480 finite elements, is shown in fig. 7, and was automatically generated by COMOC from the five super element description shown in the lower half of the figure. Upon viewing the results for this discretization, a non-uniform refinement of the computational zones upstream of the leading edge was defined for COMOC (by two input number changes). This produced an approximate halving of the longitudinal span of the finite elements directly in front of the leading edge. The influence of these discretization changes on computed pressure coefficient distribution is shown in fig. 8. The addition of the coarser discretization upstream produced even poorer agreement with the reference data and the unsatisfactory "peakiness" remains. Dramatic improvement is noted for the upstream refined grid solution, even though the discretization over the airfoil remains identical to that shown in fig. 4. Some additional refinement on the leading edge region would further improve agreement at a modest increase in computer cost. Well into the upstream

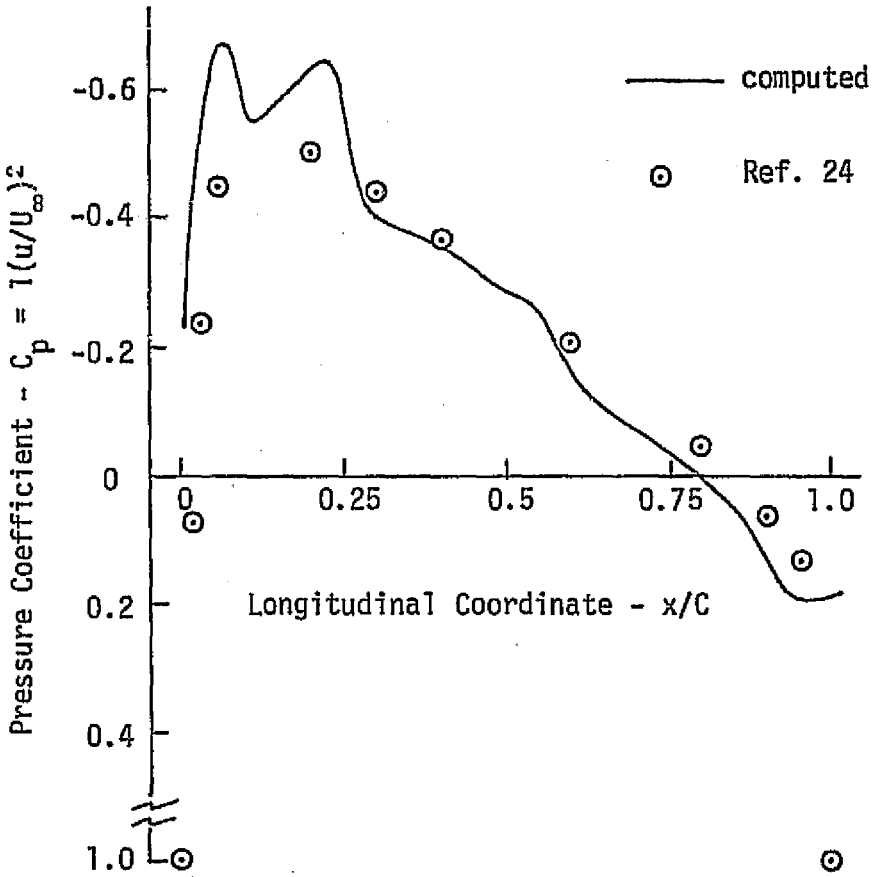

Figure 5. Computed Pressure Coefficient Distribution on NACA 0015 Airfoil.

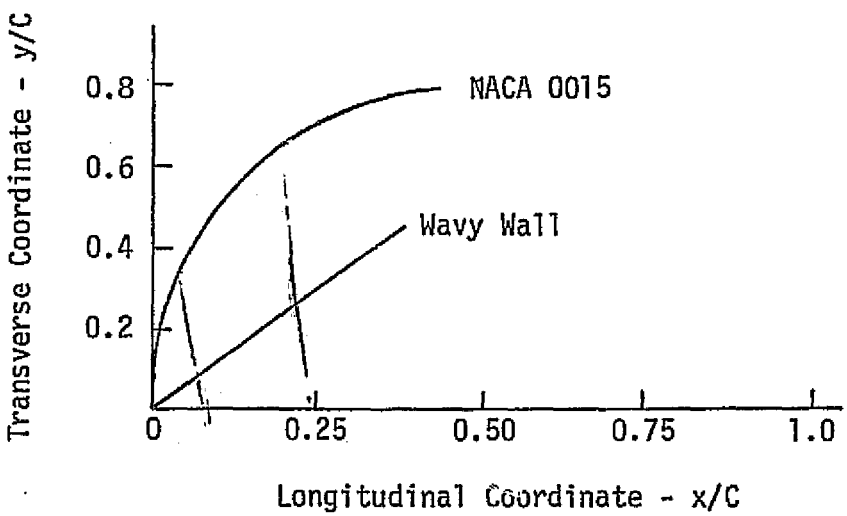

Figure 6. Leading Edge Geometries.

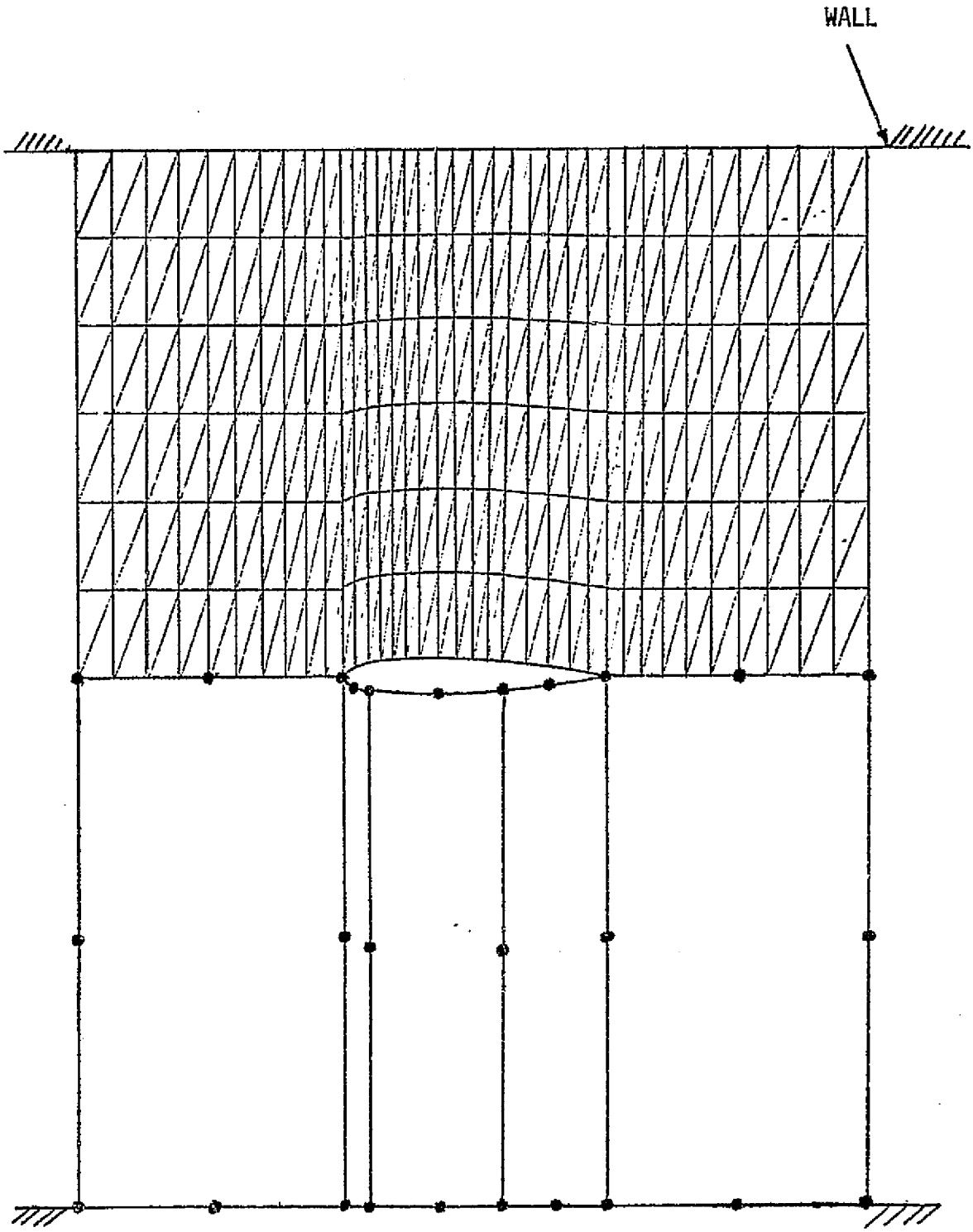

Figure 7. Expanded Finite Element Discretization for NACA 0015 Airfoil.

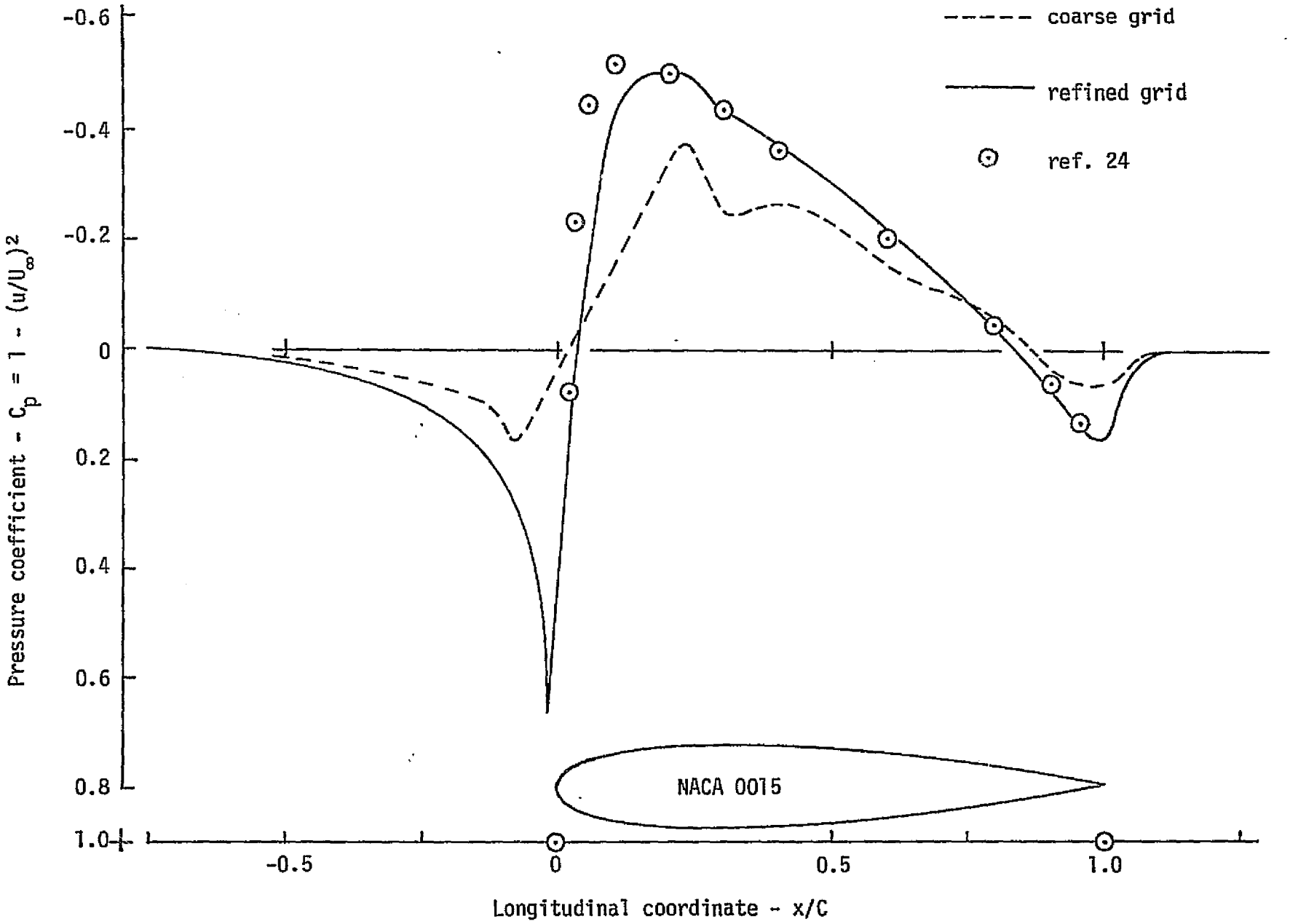

Figure 8. Computed Pressure Coefficient Distributions for NACA 0015 Airfoil.

region, note how the finite element solution anticipates the existence of the airfoil; this is the character of an elliptic boundary value problem. The refined grid solution is in excellent agreement with the reference values in the 20-95% chord region. However, note how the finite element pressure level returns to freestream immediately downstream of the trailing edge, wherein the impact of the Kutta condition on the reference solution drives the coefficient to zero. Of course, in actuality, trailing edge regions exhibit significant viscous effects. These influences effectively blunt the trailing edge for a potential flow analysis, and a specific accounting of viscous/inviscid interaction is required to accurately simulate the physics.

Alternative forms of grid manipulation exist for improving solution accuracy in leading and trailing edge regions. Global grid refinement, while effective, increases the order (size) of the solution matrix to be solved dramatically, thereby requiring more core storage. In addition, since solution time varies as approximately the square of the number of nodes, use of very fine grids is economically impractical. Local refinement can retain a manageable number of elements by employing non-uniform distributions to place smaller elements in the high velocity gradient areas. This may become quite practical, but considerable numerical experimentation is required to optimize the procedure. For highly curved surfaces, like the leading edge region, higher-order curved finite elements could be used, but their efficiency for non-linear solutions remains to be quantified (see ref. 8, 9). For low subsonic flows where density is essentially constant, deVries and Norrie (ref. 5) suggested, but did not document an alternative approach involving global refinement on a local basis. This can be accomplished by using the orthogonality properties of the potential function and streamfunction to shrink the solution domain, i.e., translate the infinity closure nearer the airfoil. This method appears promising, since the total number of nodes in the solution field remains small while establishing progressively finer grids near the airfoil. To evaluate this method, the previous case of low Mach number flow over a symmetric NACA 0015 airfoil at zero angle of attack was repetitively solved starting with the discretization shown in fig. 7. The distribution of streamfunction was first determined by solution of eqn.(40) in two-dimensional form. The results are shown in fig. 9. The $\psi = .15$ streamline

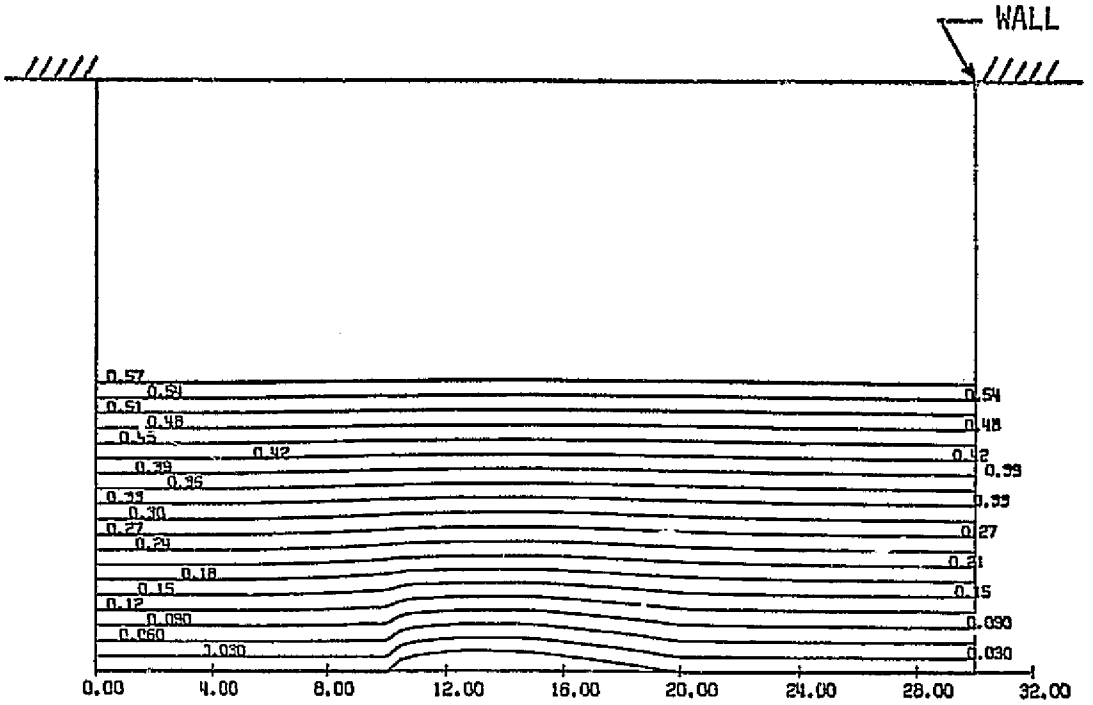

Figure 9. Initial Potential Flow Computed Streamfunction Distribution.

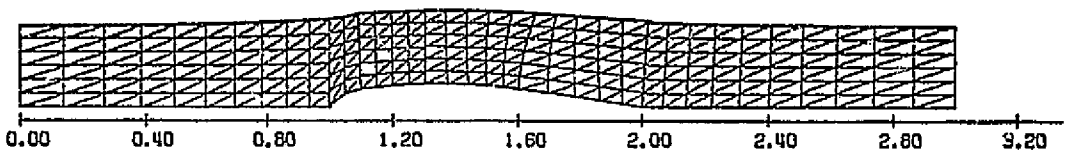

Figure 10. Refined Grid Finite Element Solution Domain for NACA 0015 Airfoil.

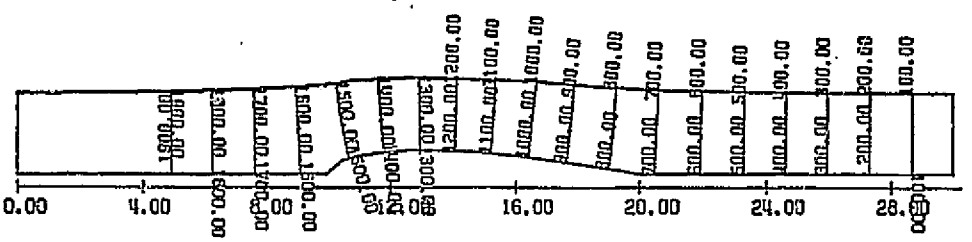

Figure 11. Refined Grid Potential Function Solution for NACA 0015 Airfoil.

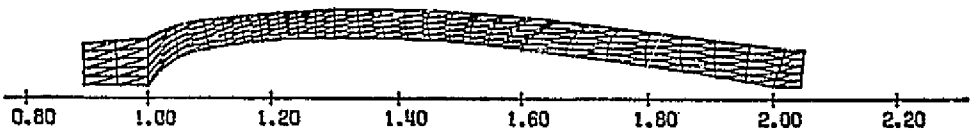

Figure 12. Second Refined Finite Element Grid for NACA 0015 Airfoil.

was then chosen as the upper boundary for the next sequential evaluation; the solution domain was rediscretized as shown in fig. 10. This discretization employs the same number of triangular finite elements as did the original, but the average finite element span has been reduced by approximately six. Figure 11 shows the computed potential solution on the reduced domain, and fig. 12 illustrates the next reduced solution domain, wherein the upstream and downstream boundaries lie on constant potential levels as computed using the discretization of fig. 11. This procedure appears to provide a viable alternative for handling infinity boundary conditions associated with external incompressible flows. However, it remains to fully assess the accuracy improvement that results in pressure coefficient distribution on the basis of cost effectiveness.

Dealing with non-symmetric airfoils and/or angle of attack requires full discretization of multiply-connected solution domains. Practical solution of these cases with lift is of ultimate importance. The major difficulties associated with these solutions is again associated with the leading and trailing edges, as well as application of the Kutta condition. To evaluate the accuracy and stability of a finite element solution, the solution domain of fig. 7 was approximately doubled in extent. The finite element discretization, obtained using a 10 super element specification, is shown in fig. 13. The discretization is purposely non-symmetric, to evaluate solution accuracy; the resultant finite element mesh contains 355 elements and 213 nodes. A visually symmetric potential distribution was computed, as shown in fig. 14. Nevertheless, the discretization produced numerical solution differences for pressure coefficient on the upper and lower surfaces, as shown in fig. 15. The maximum differences are on the order of 15%; agreement with the reference data is essentially comparable to that shown in fig. 8. A lift coefficient, C_L, was computed to determine the error induced by these differences in pressure coefficient distribution. The lift coefficient is computed by numerical integration of the upper and lower C_p levels around the airfoil as (ref. 25).

$$C_L = \frac{1}{C} \oint_C (C_{p_u} - C_{p_\ell}) d\sigma \tag{88}$$

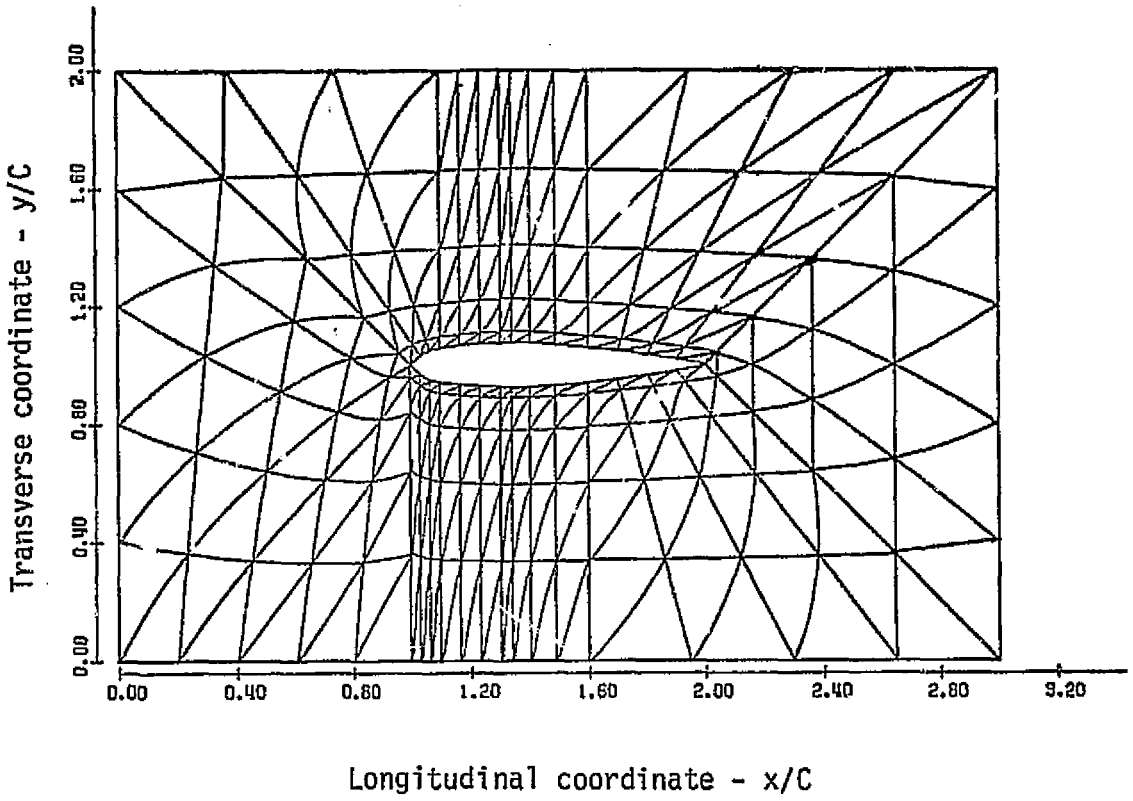

Figure 13. Complete Domain Finite Element Discretization for NACA 0015 Airfoil.

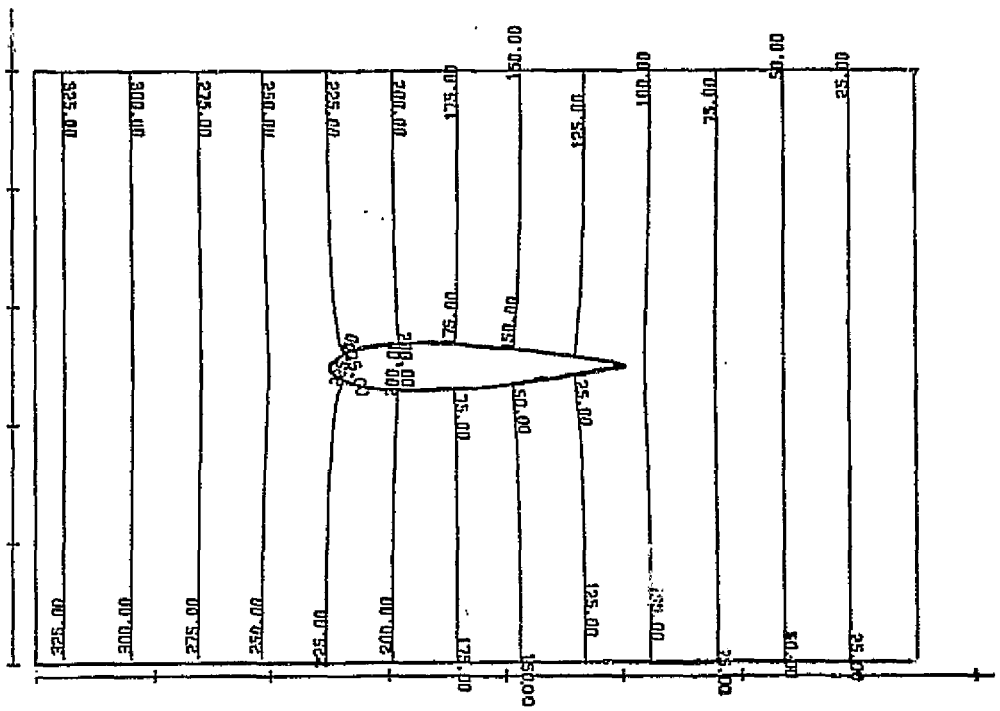

Figure 14. Complete Computed Potential Function Distribution for NACA 0015 Airfoil.

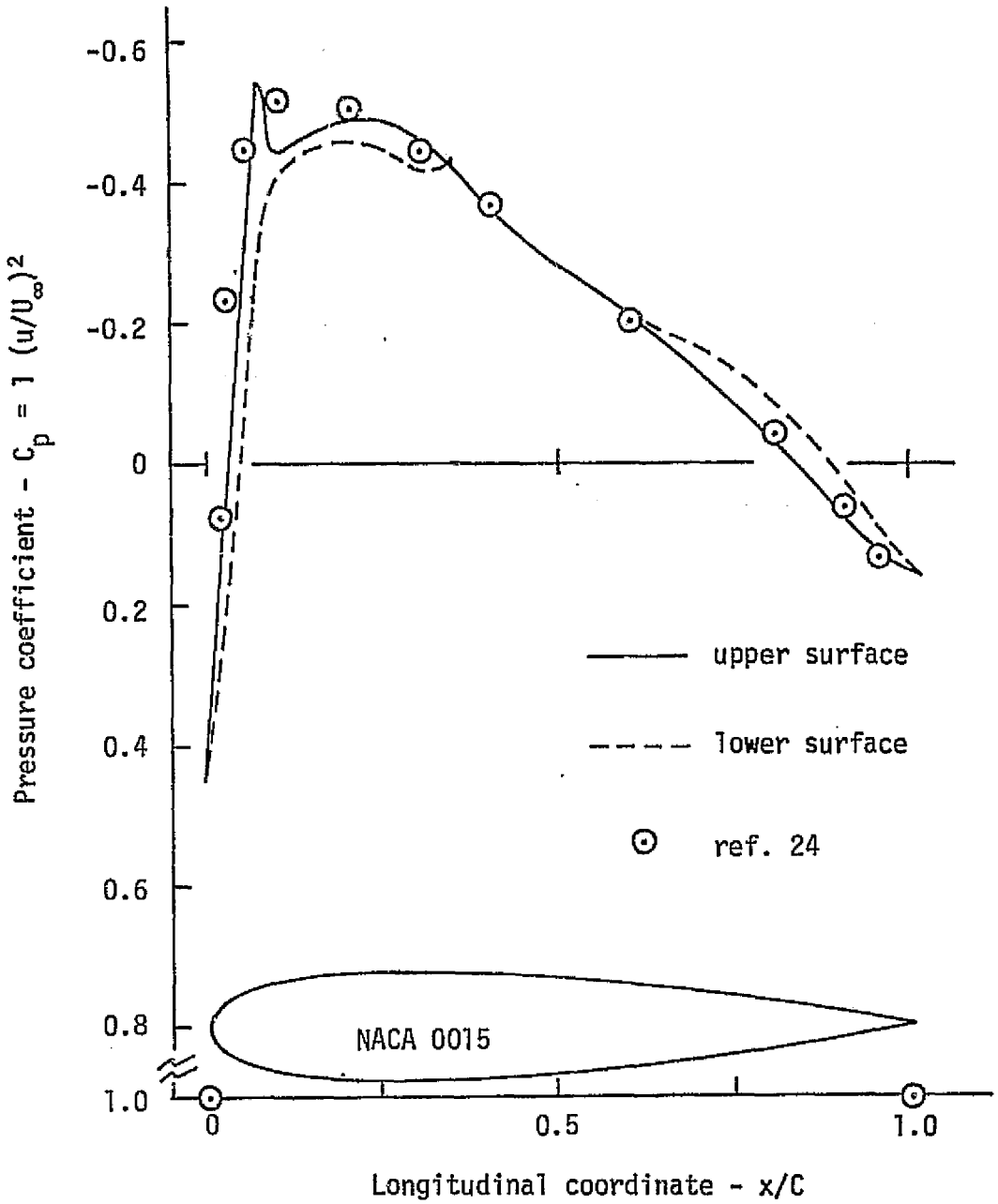

Figure 15. Variation in Computed Pressure Coefficient Distribution on NACA 0015 Airfoil Due to Non-symmetric Discretization.

The resulting C_L determination for the NACA 0015 airfoil, at zero angle of attack, see Table 2, is -.00276, or an effective attack angle of -.02° . These results tend to indicate the acceptable accuracy in lift coefficient can be achieved using coarse and skewed discretizations. This is quite important, since for nonsymmetric shapes at angle of attack, it is essentially impossible to maintain a symmetric discretization. The magnitude of the error in C_p, hence C_L , is directly associated with discretization fineness; as previously demonstrated, it can be controlled through grid refinement.

Table 2. Pressure Coefficient Distribution on NACA 0015 Symmetric Airfoil at Zero Angle of Attack, Non-Symmetric Finite Element Grid

x	C_{p_u}	C_{p_ℓ}	$C_{p_u}-C_{p_\ell}$	Δs	$\frac{1}{C}\int (C_{p_u} - C_{p_\ell})d\sigma$
1.0	.380	.380	0.	0.	0.
1.0333	.035	.180	-.145	.0333	-.00240
1.0667	-.517	-.298	-.101	.0333	-.00410
1.1	-.442	-.416	-.030	.0333	-.00218
1.1667	-.473	-.461	-.012	.0667	-.00141
1.2333	-.491	-.448	-.043	.0667	-.00183
1.3	-.444	-.425	-.019	.0667	-.00210
1.338	-.440	-.444	.004	.038	-.00028
1.4	-.364	-.368	.004	.062	.00025
1.488	-.291	-.292	001	.088	.00022
1.6	-.210	-.213	.003	.112	.00022
1.7	-.128	-.164	.036	.1	.00200
1.8	-.033	-.096	.063	.1	.00495
1.9	.075	.012	.063	.1	.00630
2.0	.145	.145	0.	.1	.00320

$C_L = -.00276$

As an example for an unsymmetric flow, the airfoil of fig. 13 was rotated to 15° angle of attack, and solution domain automatically discretized, as shown in fig. 16. The ability of the finite element procedure to use such non-uniform discretizations now becomes a distinct feature; the capability to produce them automatically can reduce user input effort by several orders of

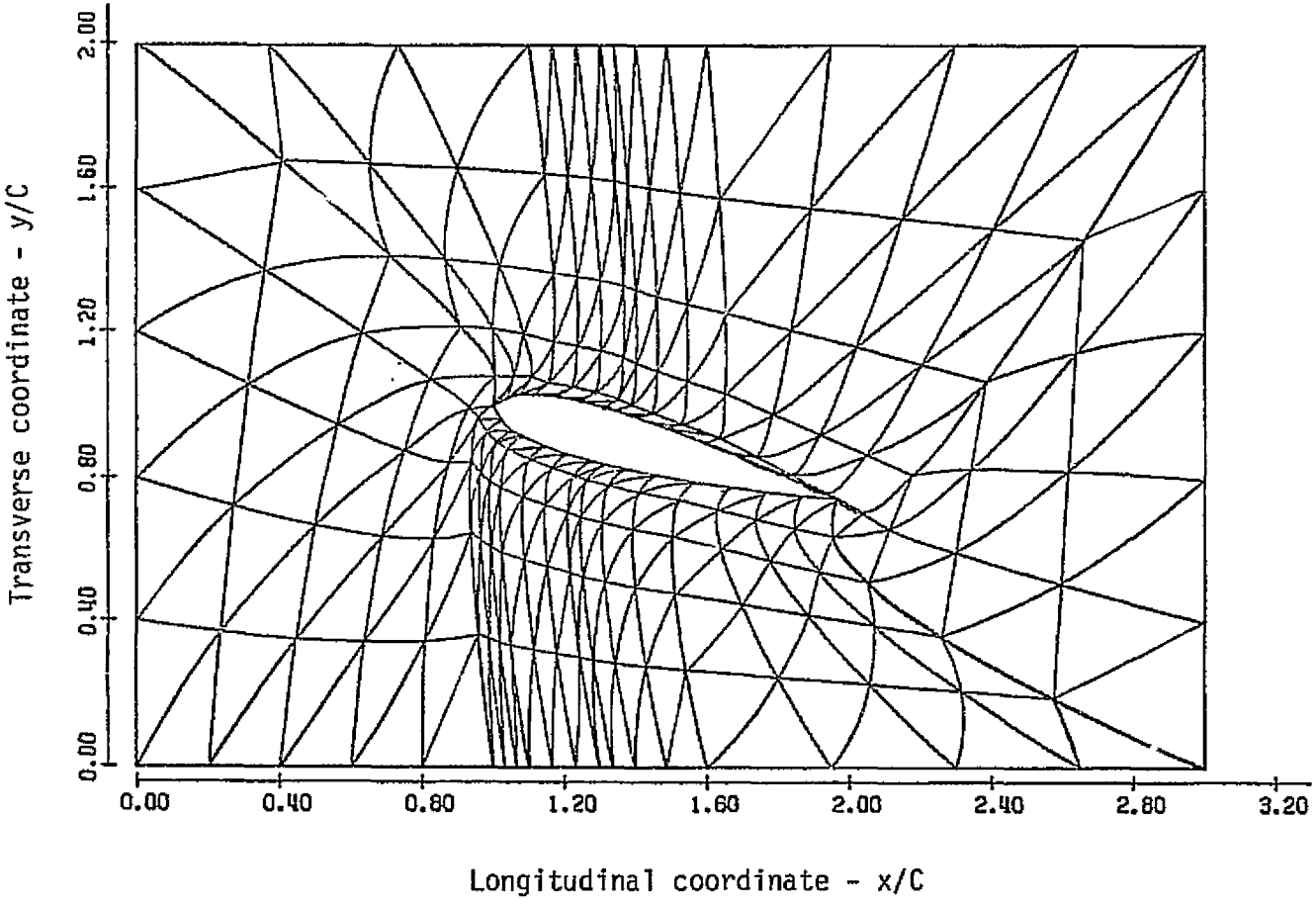

Figure 16. Complete Domain Finite Element Discretization for NACA 0015 Airfoil at 15° Angle of Attack.

magnitude. As embodied in COMOC, automatic refinement of minimal data input is accomplished over arbitrary geometric shapes. The algorithm involves quadriatic functional representation over one, two and three-dimensional finite element spaces, using natural coordinate descriptions of the serendipidity finite element family (ref. 26). For the two-dimensional problems considered herein, the user-specified super elements are general triangular or quadrilateral shapes, which may have curved sides not containing points of inflection. Any two-dimensional domain or series of domains can be discretized by decomposition into quadrilateral and triangular shapes and specifying the number and type of elements to be generated in each. The level of user input effort can be even further reduced when geometric similarity of boundary regions exists for a class of problems. Airfoil analysis at various angles of attack in an unbounded stream exhibits such a similarity which can be exploited. To illustrate the general case, consider the sequence in fig. 17. Uniform inflow conditions are specified at the left end of the rectangular (or any other shape) box of fig. 17a. A vanishing normal gradient is appropriate along the top and bottom streamlines, while at outflow, proper surface orientation allows specification of constant potential. The airfoil shape, see fig. 17b, is input as specification of mean line coordinates and thicknesses. From these two specifications, super element coordinate data can be generated in a predetermined fashion for angle of attack, see fig. 17c-d, to serve as automatic discretizer input data. The addition of flaps or slats is conceptually straightforward; options could be added to the super element generation routine to allow their specification in terms of chord line coordinates, thickness distribution, and angle of attack. The combining of these techniques, coupled with automatic setting of the domain boundaries along lines of constant streamfunction and potential function, can provide a powerful, rapidly accessible and reliable tool for finite element analysis of general airfoil configurations.

Aerodynamic Viscous Flow Solutions

As indicated earlier, for conventional aerodynamic flows at low angle of attack, the inviscid flow field is separated from the airfoil by a generally thin region dominated by viscous effects. Therefore, the solution of the

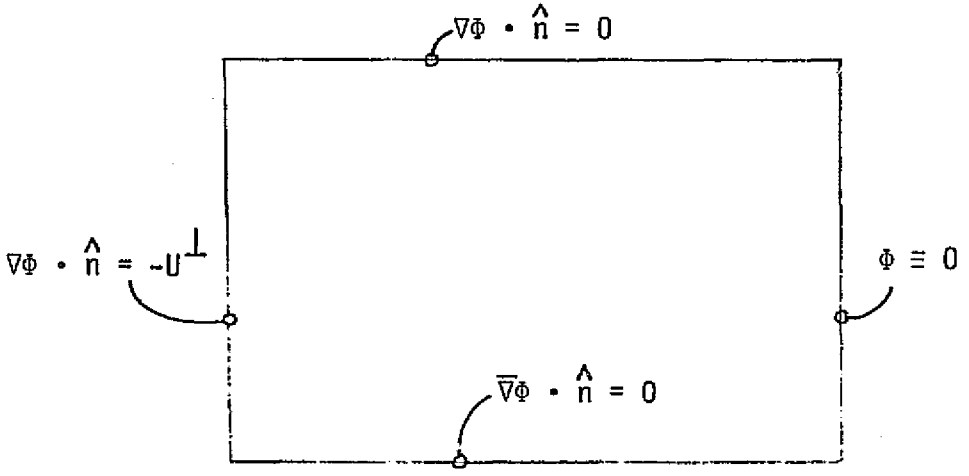

a) Infinity Boundaries (f(t))

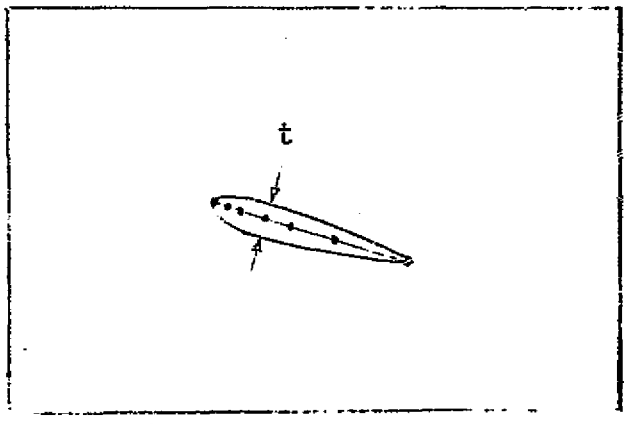

b) Airfoil Description

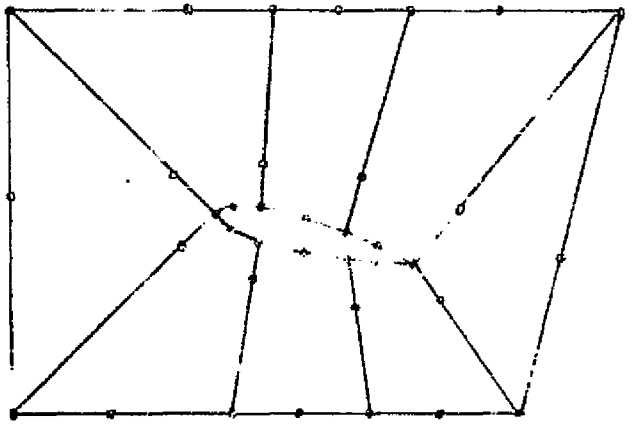

c) Automatically Generated Initial Super Element Discretization

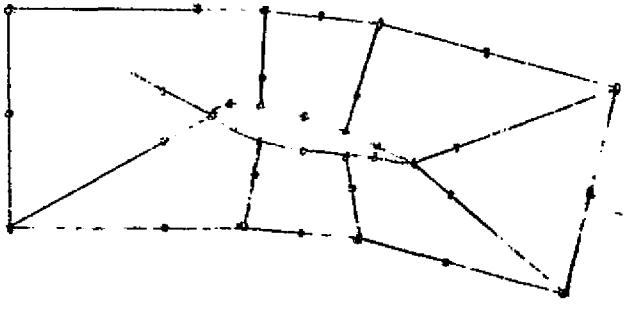

d) Automatically Generated Streamline Super Element Discretization

Figure 17. Automated Finite Element Discretization for Potential Flow Analysis.

two-dimensional boundary layer equations is an important requirement for computational simulation, and is readily accomplished within the developed Navier-Stokes Variant of COMOC. Since this computer program assumes all "parabolic" flows are three-dimensional, the dimensional-degeneracy of two-dimensional flow is obtained by employing a single column of finite elements spanning the boundary layer thickness, see fig. 18. The discretization extends into the freestream, where the inviscid flow is matched by a vanishing gradient boundary condition. The wall is assumed no-slip, and the lateral vanishing gradient boundary conditions yield the desired two-dimensional simulation. The character of the finite element solution of eqn.(45)-(49) can be evaluated for accuracy and convergence by comparison with solutions produced by finite-difference techniques and with a similarity solution for constant specific heat. The check case corresponds to a nominal Mach 5, laminar, two-dimensional, air boundary-layer flow over an adiabatic wall in a favorable pressure gradient. With the assumption of constant specific heat, the flow is isoenergetic and it is necessary only to solve the x_1 momentum equation and the continuity equation. The initial distribution for longitudinal velocity u_1 is established from the similar solution for $\beta = 0.5$ and $S = 0$ (ref. 27). The initial distribution for u_2 is obtained iteratively, and Sutherland's law is employed to compute viscosity.

The test case is initialized at $x_1 = 0.03$ m downstream from the leading edge. The boundary-layer thickness at this station δ_0 is 0.0039 m , the local Mach number M_e is 3.77 , the Reynolds number R_e is 0.83×10^5 per meter, and the adiabatic wall temperature T_w is 1000 K . Shown in fig. 19 are the computed distributions of skin friction, local free-stream Mach number, and boundary-layer thickness for the case of constant specific heat. These were obtained with two uniform finite-element discretizations corresponding to four and eight elements spanning the initial boundary-layer thickness, see fig. 18. The static pressure distribution $p_e(x_1)$ is also presented for reference. The boundary-layer thickness has increased more than fourfold within the solution. Only small differences, on the order of about 2 percent, exist between the two solutions, the finer discretization producing a slightly larger skin friction and smaller local Mach number. Superimposed for comparison purposes are the results for the similar solution (ref. 27) and a 20-zone

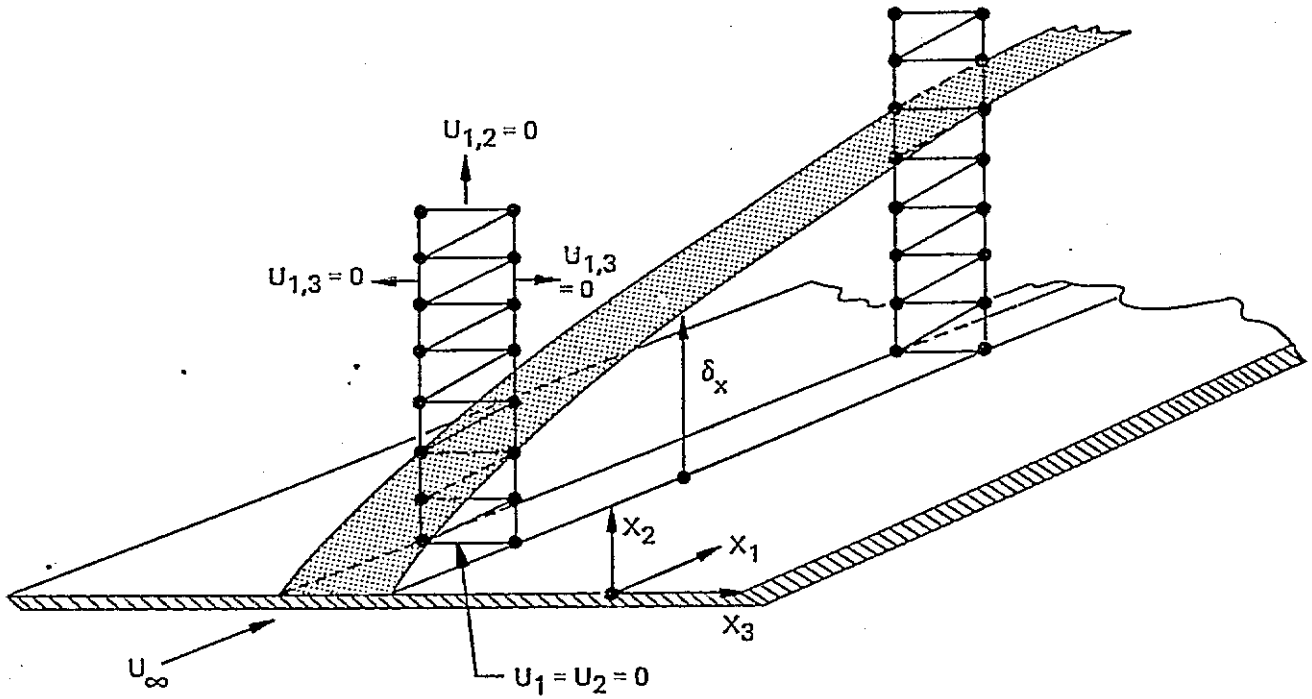

Figure 18. Finite Element Discretization for Two-Dimensional Boundary Layer Flow.

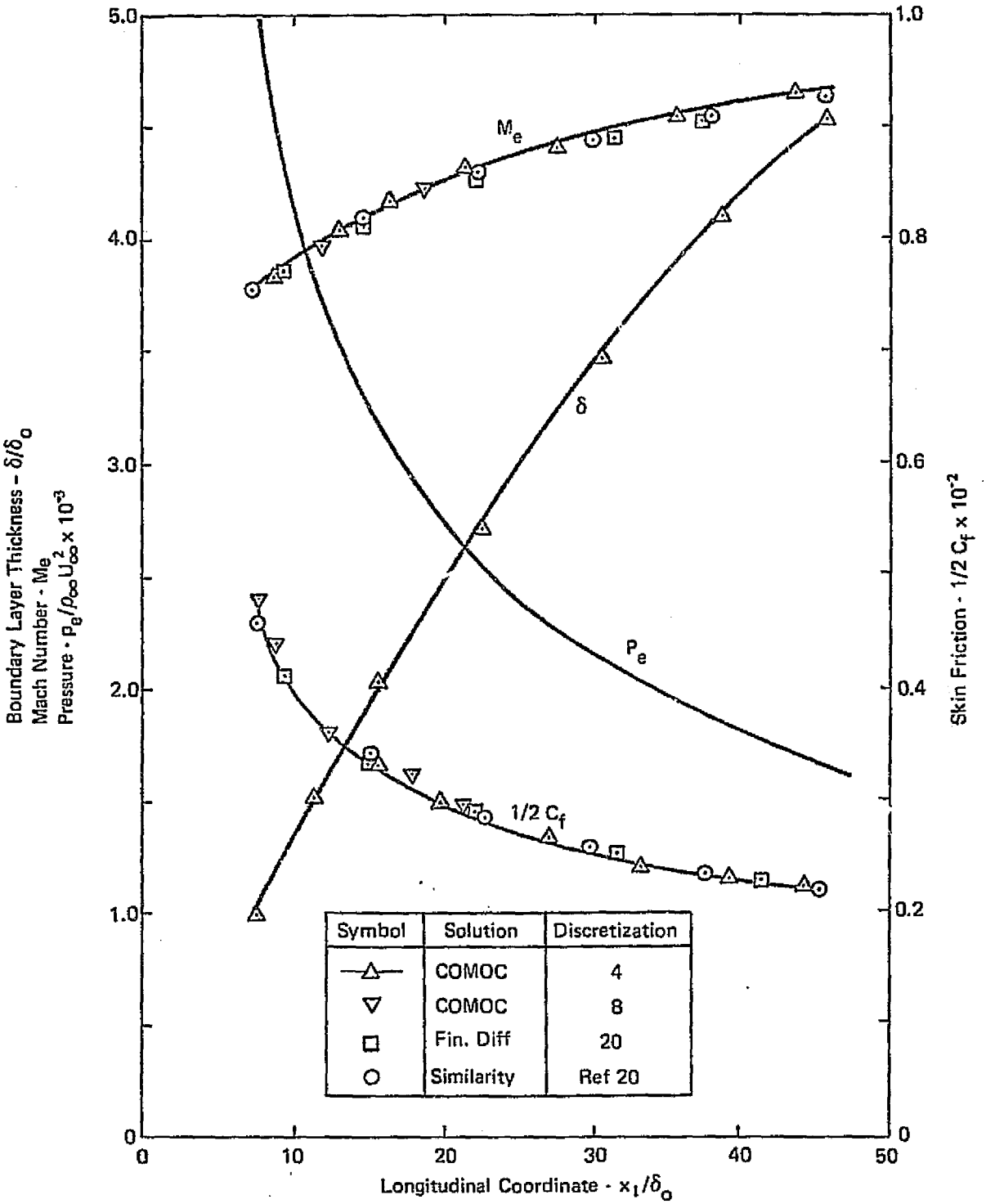

Figure 19. Computed Supersonic Boundary Layer Parameters, M = 5, Re_x = .83(5)/m, β = 0.5.

finite-difference solution obtained with the Von Mises coordinate transformation. Agreement among the four solutions is excellent (within 2 percent) for skin friction. The similar solution for M_e lies between the COMOC and finite-difference solutions, and overall agreement is within ± 3 percent.

Shown in fig. 20 are computed velocity profiles at $x_1/\ell_0 = 22.7$, which is about midway through the presented solution. For reference purposes, the initial longitudinal velocity profile is given with the node locations of the four-element discretization superimposed. Both finite element solutions produce u_1 distributions that are slightly more concave upward in the midregion in comparison with the similar or finite-difference solution. The eight-element COMOC solution lies closer to the similar solution in the region where the two finite element solutions differ. The finite-difference solution lies appreciably below both the COMOC and similar solutions near the free stream. The computed transverse velocities, which are also plotted in fig. 20, show only slight differences between the two discretization solutions. The trends of the COMOC solutions are in excellent agreement with the established precedures; unfortunately, since each method of solution is distinctly numerical, no absolute accuracy assessment is established. However, for an incompressible boundary-layer flow, absolute accuracy and convergence rates for the finite-element solution have been established to be close to theoretically predicted values (ref. 14, 28).

As noted in the discussion of potential flow solutions on a NACA 0015 airfoil, the computed pressure coefficient distribution (see fig. 8) indicates the (inviscid) surface velocity is retarded by an adverse pressure gradient on the interval $0.20 \leq x/C \leq 0.99$. Along the interval $0.85 \leq x/C \leq 0.99$, the computed velocity is below the reference freestream value. The finite element solution computed a local acceleration, immediately downstream of the trailing edge, sufficient to return the surface flow to equilibration with the freestream. Of course, viscous effects would significantly modify these perfect fluid results. The merging flow phenomena in the trailing edge region can be particularly complex, and a thorough computational analysis could be of considerable value, especially with regards to overall drag prediction. The finite element algorithm for solution of the boundary layer equations (45)-(49) merging into a parabolic Navier-Stokes equations (57)-(59) solution was

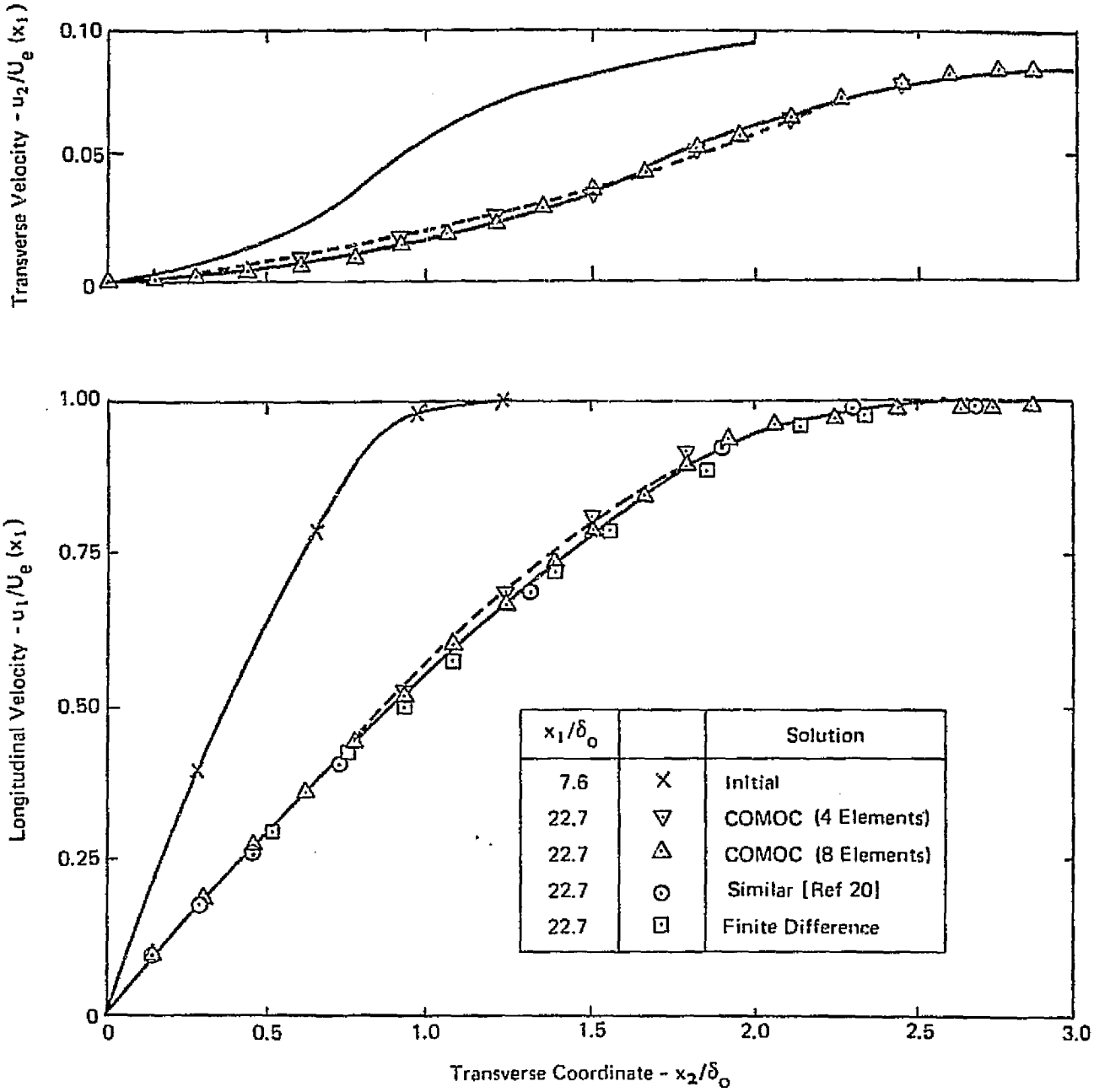

Figure 20. Computed Supersonic Boundary Layer Velocity Distributions, $M = 5$, $Re_x = .83(5)/m$, $\beta = 0.5$.

evaluated by COMOC. As the first step towards an airfoil trailing edge simulation, arbitrarily different, laminar boundary layer flows were allowed to develop on both sides of an infinitely thin flat plate. The plate was then computationally terminated, and the two boundary layer trailing edge velocity profiles (u_1 and u_2) were allowed to merge within a single, unbounded solution domain. The test case corresponds to (essentially) constant density, isoenergetic flow of air at a nominal Mach number of 0.27 and a reference freestream velocity, $U_\infty \approx 30$ m/s . The finite element discretizations appear similar to that presented in fig. 18, (on both the top and bottom sides of the surface) and were of sufficient fineness to maintain ±1% solution accuracy on prediction of u_1 .

Initially, consideration was given to continued use of the boundary layer equation system downstream of the merging of identical upper and lower velocity profiles. Inconsistencies in the differential equation description were immediately encountered for u_2 , however. As described in the theoretical development section, the boundary layer equations cast solution for u_2 on an initial-value specification starting at the solid surface. This surface vanishes from the solution domain, immediately upon flow field merging downstream of the plate termination. Since the flow from the plate to the unbounded region is (assumed) smoothly continuous, in the latter the solution for u_2 must become a two-point boundary value problem (in two-dimensional space). This is possible only by retention of the x_2 momentum equation for solution of u_2 , and combining the continuity and vector momentum equation to yield an appropriately deterministic form for pressure prediction, see eqn.(62)-(66). Computational experimentation using COMOC confirmed these theoretical musings. It was indeed impossible to obtain smooth transition from the boundary layer u_2 distributions while maintaining consistency of the freestream values.

These early results actually led to extension of COMOC to switch over to the appropriate parabolic Navier-Stokes system while undergoing a restart. For ensuing simulations, dissimilar upper and lower surface boundary layer profiles were allowed to develop from an initial slug (uniform) profile. Such a starting procedure minimizes input preparation; the boundary layer velocity profile that developed 1.2 m downstream of the simulated leading edge

agreed within ±1% of the Blasius solution at 1.0 m downstream at the same Reynolds and Mach numbers. Hence, arbitrarily dissimilar boundary layer profiles were readily obtained to initiate the parabolic Navier-Stokes solutions. At restart, all program parameters used by COMOC to control integration were reset to their initial values. The two previously separate boundary layer solution domains were merged by adding the node at the plate into the integration array, and specifying vanishing gradient boundary conditions for both u_1 and u_2 everywhere about the closure of the newly defined domain. Initial evaluation for identical upper and lower initial velocity profiles showed that the COMOC-predicted results for u_1 and u_2 remained exactly symmetric to five significant digits for merged solution domains up to 1.3 m long. The axial pressure gradient, computed using a pressure algorithm for eqn.(63), vanished to within 0.5% on U_∞. The skew-symmetry on u_2 was exactly preserved; the null value remained on the downstream projection of the plate throughout the solution. Subsequent evaluations utilized dissimilar upper and lower velocity profiles. The results of one such computation are shown in fig. 21. The plate terminus boundary layer initialization profiles are shown for $x_1/\delta_0 = 267$; other profiles are shown for various stations downstream of the trailing edge. Due to the original dissimilarity of the initial velocity profiles, note that the locus of the velocity profile minimum is concave upwards, yielding a modest overall curvature in the merged flow field. For this case also, the computed axial pressure gradient, eqn.(63), vanished to within 0.5% on U_∞ . The lateral pressure gradient was assumed to vanish identically. For non-flat plate flows, both axial and lateral pressure gradients can be induced by flow field curvature. Their computational prediction requires embodiment and check-out of solution algorithms for the various pressure descriptors, eqn.(65)-(66).

Computational predictions in laminar wakes are of limited interest in practical aerodynamics; the prime value of the discussed results is identification of appropriate equation systems and proof of computational stability. Even at low angle of attack, the initial laminar boundary layer flow will typically undergo transition and become fully turbulent before the trailing edge is reached. Hence, a far more practical computation for simulated airfoil wake flow would involve specification of a turbulent

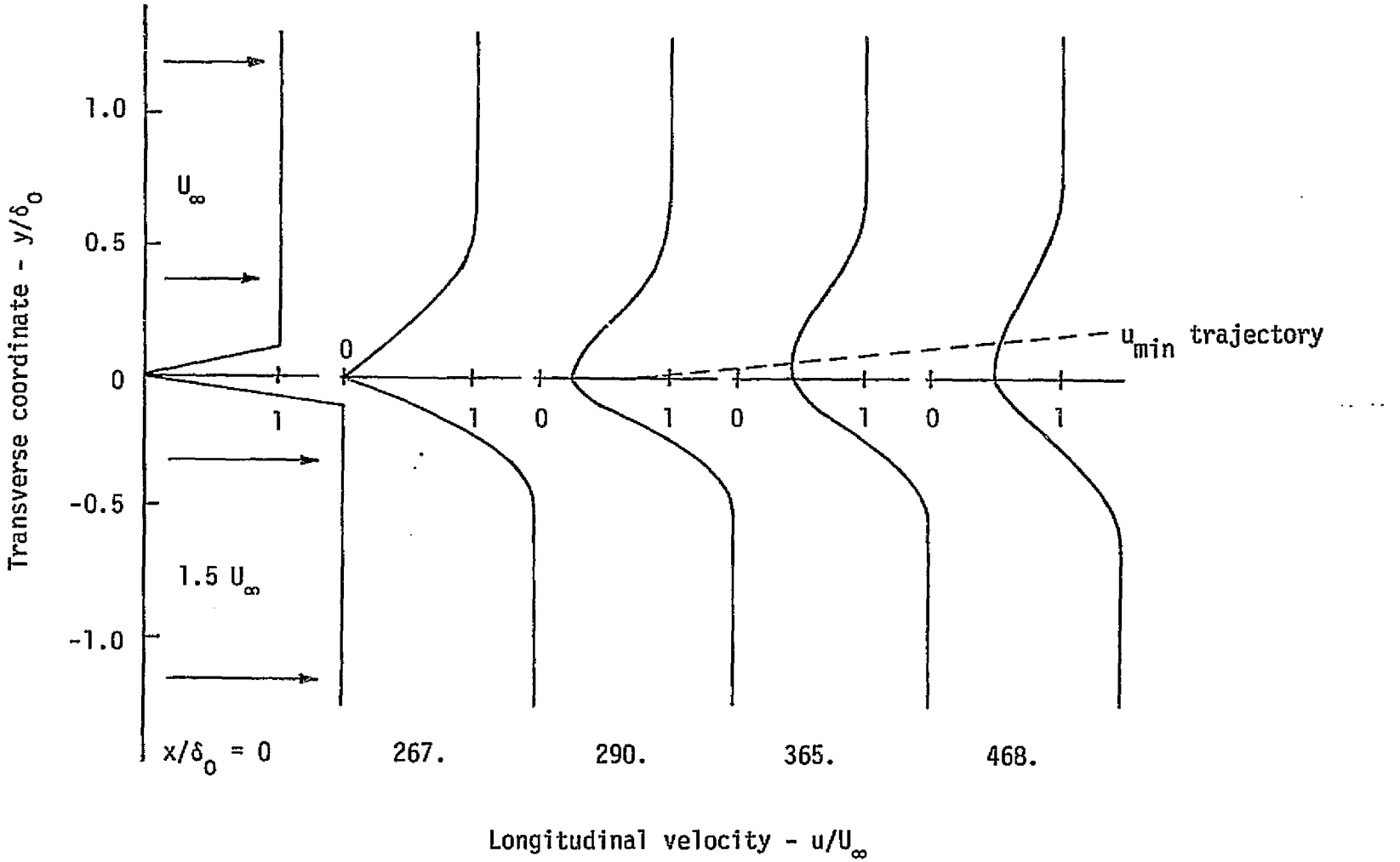

Figure 21. Dissimilar Laminar Boundary Layer Merging Downstream of a Trailing Edge.

closure relation, eqn.(5), for solution of eqn.(45)-(48) and/or eqn.(57)-(58). Conventional turbulent boundary layers can be effectively predicted using a mixing length hypothesis (cf., ref. 29), wherein

$$\epsilon_{12} \equiv \ell^2 |u_{1;2}| \tag{88}$$

In eqn.(88), ℓ is the mixing length conventionally defined as

$$\ell \equiv \begin{cases} k\ x_2 \omega & 0 \leq x_2 \leq \lambda\delta/k \\ \lambda\ \delta\ \omega & \lambda\delta/k < x_2 \end{cases} \tag{89}$$

where typically, $k = 0.435$, $\lambda = 0.09$, δ is the boundary layer thickness, and ω is the Van Driest damping coefficient, used to smoothly merge eqn.(88) into the sublayer molecular kinematic viscosity. An alternative approach, of general applicability throughout multi-dimensional fluid mechanics, involves formation of the turbulent kinetic energy of the flow, and a closure hypothesis involving a suitable length scale (cf., ref. 18). Employing an order of magnitude analysis (cf., ref. 30), the turbulent kinetic energy is a point function which satisfies the same general partial differential system, eqn. (76)-(79), for which the finite element solution algorithm has been established. The required length scale can also be determined from solution of a differential equation (for example, from the dissipation function), or be hypothesized directly for geometrically simple flows. Results for finite element prediction of turbulent three-dimensional boundary region flows, using both closure techniques and COMOC, are reported in refs. 31-32. These results indicate that extension of the finite element methodology to multi-dimensional turbulent flows, of impact in trailing edge wake flow predictions, will be directly accomplished.

The final aerodynamic problem class, for which the finite element solution procedure has been evaluated, corresponds to highly rotational vortex flows. Two problem classes of immediate potential applicability include, 1) analysis of the persistence of trailing vortex streets as generated by the lift distribution along highly loaded airfoil configurations typical of current wide-body jets, and 2) prediction of the penetration and turbulent decay of high energy jet flows injected non-tangentially into a crossflow as might occur in thrust vector control for VTOL aircraft. In each case, the

vortex structure will decay as a function of time and the local effective diffusion and convection effects. The vortex center will move as a function of cross flow velocity, initial strength and direction, and the magnitude of the tangential velocity at the juncture of contra-rotating vortex pairs. A complete numerical simulation typically requires solution of the full form of the Navier-Stokes equations. A cursory evaluation of the finite element solution procedure has been explored for the second problem. An initially circular jet, injected subsonically and non-parallel into a cross wind, is structured as a contra-rotating vortex pair (cf., ref. 33). For sufficient dynamic pressure, the jet penetrates into and eventually turns parallel to the impressed crossflow. The jet vortex structure provides the "elastic stiffness" essential for the impressed flow to pass around the initial jet as if it was a aerodynamic stream tube. As the jet turns and travels downstream, the impressed crossflow influences the dissipation of the initial highly-rotational structure by convection and diffusional processes.

Determination of a streamtube structure, as a function of initial vortex strength and assumed crossflow, was made using COMOC, by modeling the three-dimensional problem as a transient two-dimensional configuration described by the Navier-Stokes system written on streamfunction and vorticity, eqn.(69)-(70). A sketch of the two-dimensional vortex structure is shown in fig. 22a; the indicated counter-rotation deflects an onset flow, directed anti-parallel to the x_2 coordinate direction, around the centroidal region. The smoothed distribution of vorticity along the horizontal symmetry plane is shown in fig. 22b. For the computational simulation, this was replaced by point sources of vorticity set equal to $\pm\omega_o$ appropriately located at $x_1 \equiv \pm x_o$. Existence of the mirror symmetry plane, $x_1 = 0$, combined with use of a "sufficiently large" solution domain allows specification of vanishing vorticity everywhere on the selected domain closure for solution of eqn.(70). The mirror plane is also a streamline, as is the right side boundary in fig. 22a. The value of streamfunction taken on the latter is determined by the specified magnitude of the impressed crossflow, assumed anti-parallel to the x_2 axis at inflow (only). The resultant solution of eqn.(69) for streamfunction determines the actual inflow and outflow velocity distributions with use of the vanishing gradient (parallel flow) boundary condition for streamfunction,

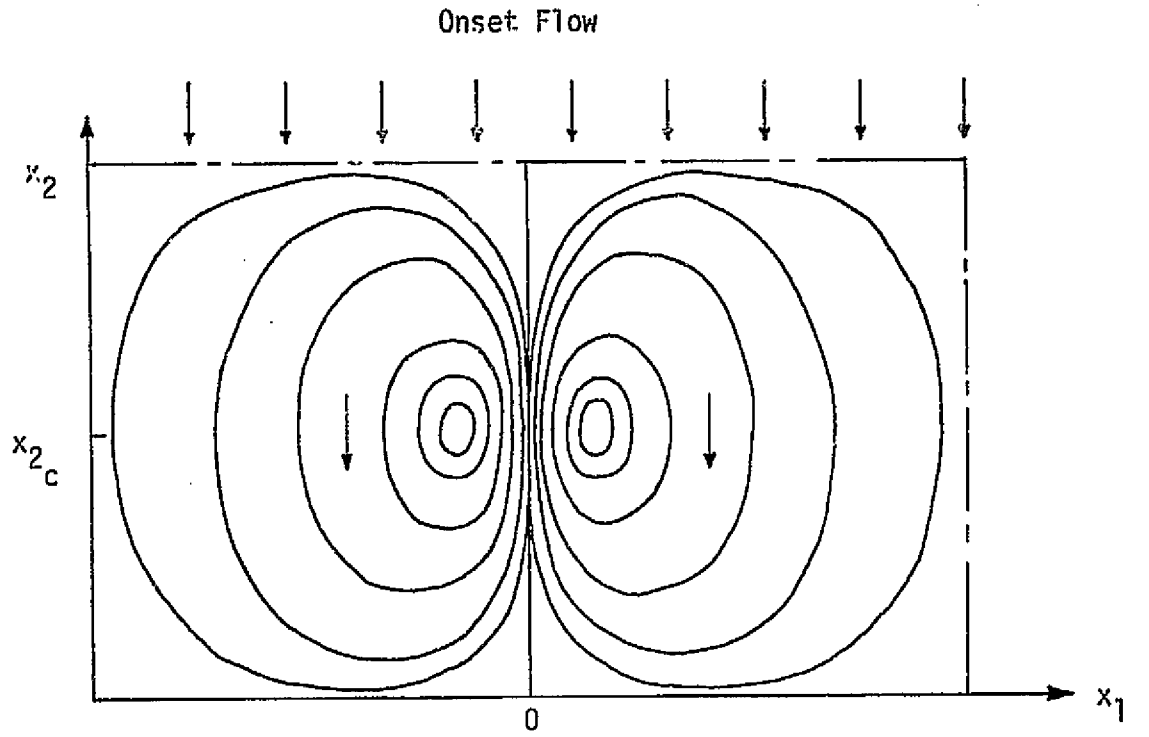

a) Two-Dimensional Counter-Rotating Vorticity Distribution

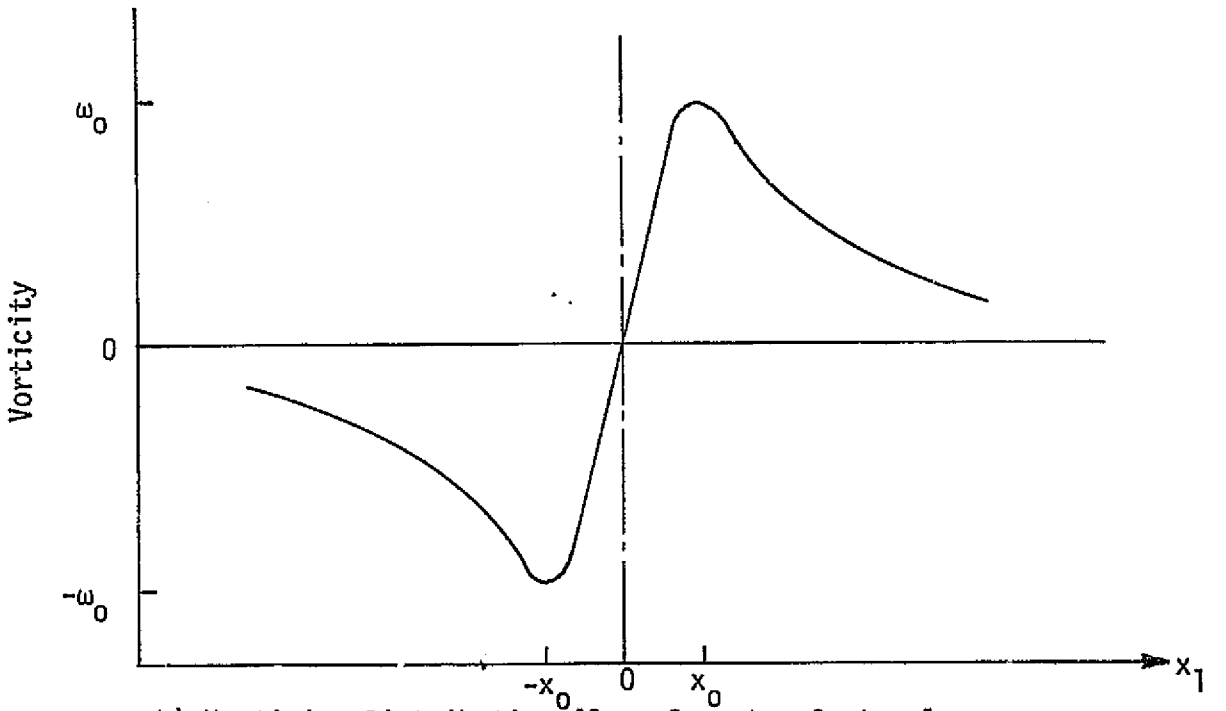

b) Vorticity Distribution Along Symmetry Centerplane, x_{2_c}

Figure 22. Vortex Structure for a Jet in a Cross Flow.

$a^{(1)} \equiv a^{(3)} \equiv 0$, eqn.(78). With these imbedded symmetry properties, only one-half the domain shown in fig. 22a is required for determining a solution; the right half was discretized using 200 triangular-shaped finite elements and 121 nodes. The cavity was presumed filled with air initially at rest, and the single vortex pair, of variable strength, was located at $x_1 = \pm 20\%\ h$, where h is the half-width domain span, fig. 22a.

Shown in fig. 23 are the COMOC computed distributions of inital mass flow within and through the solution domain for three specified values of initial vorticity, ω_0 . The displacement effect of the point source is graphically apparent. For zero specified crossflow, the computed initial streamfunction forms closed contours, as shown in fig. 24 for different initial locations for the vortex pair. (The spurious wiggles result from use of high order spline fits to sparse data by the plot package.) A continued solution of eqn.(69)-(70), to predict the decay of the initial point vortex pair, requires specification of an appropriate turbulence closure relation, eqn.(5). An accurate simulation would also require that the impressed crossflow be time varying. This would be readily accomplished in COMOC by altering the value of streamfunction on the right closure segment, fig. 23, as a specified function of time.

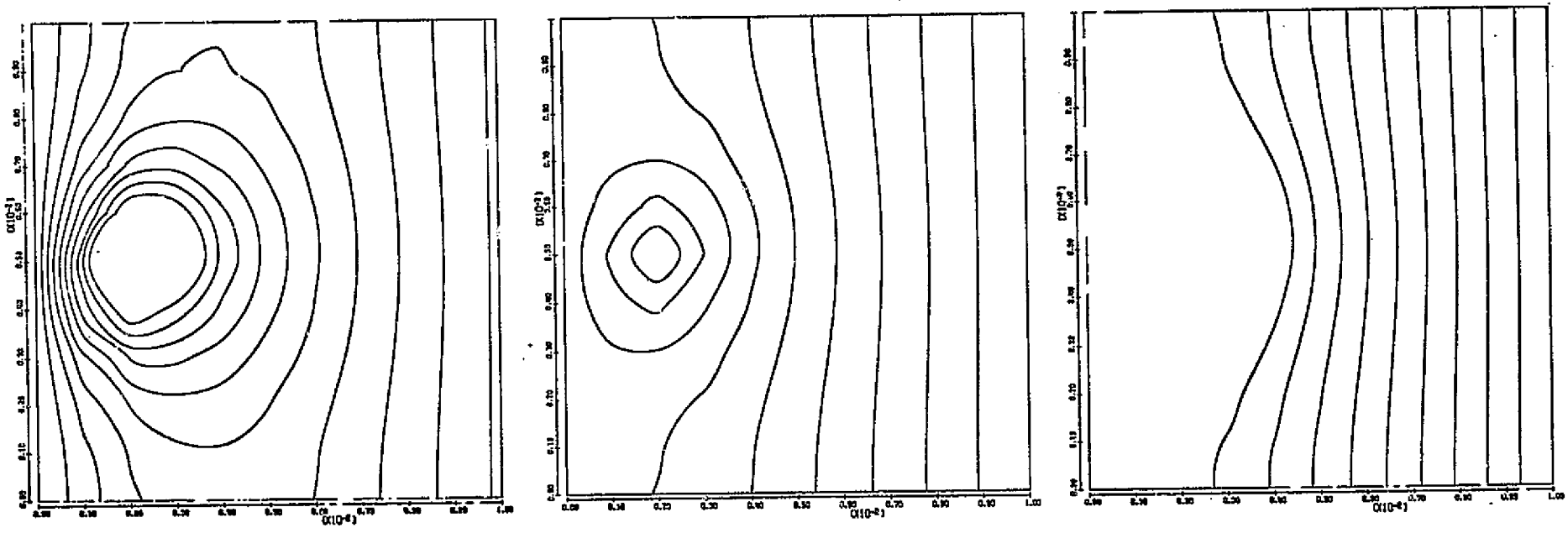

a) $\omega_o = -10^8$ b) $\omega_o = -10^6$ c) $\omega_o = -10^4$

Figure 23. Initial Streamfunction Distributions for Cross Flow Onto a Point Vortex Pair.

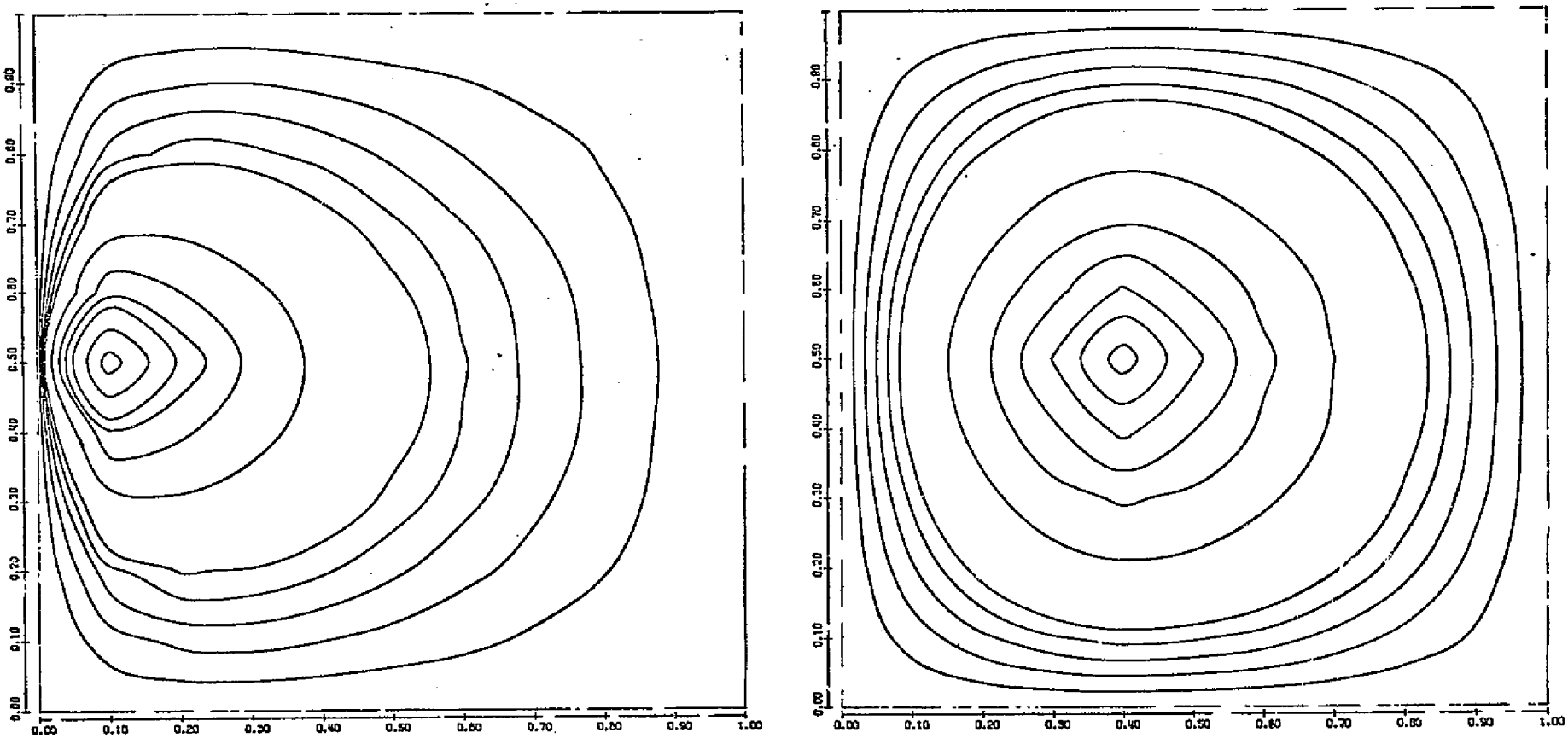

a) $x_c = 0.1$

b) $x_c = 0.4$

Figure 24. Initial Streamfunction Distributions for a Point Vortex With No Cross Flow.

CONCLUSIONS

The theoretical and computational results of this study, on application of finite element solution methodology to configuration analysis in low speed aerodynamics, indicate significant potential for the procedure. The approach taken has established appropriately complete (i.e., non-linear) differential equation descriptions for the several distinct fluid flow problem classes of impact in aerodynamics. The developed finite element algorithm is universally applicable to each description. The developing COMOC computer program, which embodies this algorithm, has verified the overall concept of a powerful, versatile general-purpose code for computational low speed aerodynamics. The generated numerical solutions in inviscid potential flow have introduced and evaluated various techniques for error control within the constraints of computational and input-requirement economics. Diverse viscous flow predictions, including a transition of differential equation system during a problem solution, indicate broad-base applicability of the algorithm and its computational embodiment. Continued progress on development of appropriate pressure solution algorithms for parabolic flows, coupling of the inviscid and viscous solutions, and expanded input/output graphics should yield a highly useful, versatile and user-oriented design tool to supplement and supplant detailed wind tunnel evaluation of complex low-speed aerodynamic systems.

REFERENCES

1. Turner, M. J., Clough, R. W., Martin, H. C., and Topp, L. J., "Stiffness and Deflection Analysis of Complex Structures," J. Aero. Sci., 23, p. 805-823, 1956.

2. Goldstein, Herbert, Classical Mechanics, Addison Wesley, USA, 1959.

3. Zienkiewicz, O. C., The Finite Element Method in Engineering Science, McGraw Hill, London, 1971.

4. Zienkiewicz, O. C. and Cheung, Y. K., "Finite Elements in the Solution of Field Problems," The Engineer, Sept. 1965, p. 507-510.

5. deVries, G. and Norrie, D. A., "The Application of the Finite Element Technique to Potential Flow Problems," Trans. ASME, J. App. Mech., Dec. 1971, p. 798-802.

6. Meissner, Udo, "A Mixed Finite Element Model for Use in Potential Flow Problems." Int. J. Num. Mtd. Engr., 6, p. 467-473, 1973.

7. Sarpkaya, T. and Hiriart, G., "On the Analysis of Target-Type Thrust Reversers," AIAA Paper 74-519, 1974.

8. Thompson, David S., "Finite Element Analysis of Flow Through a Cascade of Aerofoils," Univ. of Cambridge Dept. of Engineering Report, CUED/A Turbo/TR 45, 1973.

9. Isaacs, Lewis T., "A Curved Cubic Triangular Finite Element for Potential Flow Problems," Int. J. Num. Mtd. Engr., 7, p. 337-344, 1973.

10. Hirsch, C. and Warzee, G., "A Finite Element Method for Flow Calculations in Turbo Machines," Free University of Brussels Report V.U.B-Str-5, July 1974.

11. Vooren, J.V.D. and Laburjere, Th. E., "Finite Element Solution of the Incompressible Flow Over an Airfoil in a Nonuniform Stream," Proceedings Int. Conf. on Num. Mtd. in Fluid Dynamics, Southampton, England, Sept. 26-28, 1973.

12. Finlayson, B. A. and Scriven, L. E., "The Method of Weighted Residuals - A Review," App. Mech. Rev., 19, No. 9, p. 735-748, 1966.

13. Bratanow, T. and Ecer, A., "On the Applications of the Finite Element Method in Unsteady Aerodynamics," AIAA J., 12, No. 4, p. 503-510, 1974.

14. Baker A. J. and Zelazny, S. W., "COMOC: Three-Dimensional Boundary Region Variant, Theoretical Manual and User's Guide," NASA CR-132450, May 1974.

15. Baker, A. J., "A Finite Element Solution Algorithm For the Navier-Stokes Equations," NASA CR-2891, June 1974.

16. Baker, A. J., "Predictions in Environmental Hydrodynamics Using the Finite Element Method, I. Theoretical Development," AIAA J., 13, No. 1, p. 36-42, 1975.

17. Chan, S.T.K., Brashears, M. R. and Young, V. Y., "Finite Element Analysis of Transonic Flow by the Method of Weighted Residuals," AIAA Paper 75-79, 1975.

18. Donaldson, C. duP., Sullivan, R. D., Rosenbaum, H., "A Theoretical Study of the Generation of Atmospheric - Clear Air Turbulence," AIAA J., 10, No. 2, pp. 162-170, 1972.

19. Jaunzemis, W., Continuum Mechanics, McMillan, New York, 1967.

20. Shames, Irving H., Mechanics of Fluids, McGraw Hill, New York, 1962.

21. Schlichting, Herman, Boundary Layer Theory, McGraw Hill, New York, 1968.

22. Patankar, S. V. and Spalding, D. B., "A Calculation Procedure for Heat, Mass and Momentum Transfer in Three-Dimensional Parabolic Flows," Int. J. Heat Mass Trans., 15, 1972, p. 1787-1806.

23. Roache, P. J., Computational Fluid Dynamics, Hermosa Publishers, Albuquerque, 1972.

24. Abbott, I. H. and von Doenhoff, A. E., Theory of Wing Sections, Dover Publications, New York.

25. Liepmann, H. W. and Puckett, A. E.,"Introduction to Aerodynamics of a Compressible Fluid," John Wiley & Sons, New York.

26. Manhardt, P. D. and Baker, A. J., "COMOC: Computational Continuum Mechanics Variant User's Guide for One Dependent Variable Systems," Bell Aerospace Company Report Number 9500-920334, December 1974.

27. Christian, J. W., Hankey, W. L. and Petty, J. S., "Similar Solutions of the Attached and Separated Compressible Laminar Boundary Layer with Heat Transfer and Pressure Gradient," ARL-70-0023, 1970.

28. Popinski, Z. and Baker, A. J., "An Implicit Finite Element Algorithm for the Boundary Layer Equations," J. Comp. Phys., in review.

29. Hinze, J. O., Turbulence, McGraw Hill, New York, 1959.

30. Nash, J. F. and Patel, V. C., Three-Dimensional Turbulent Boundary Layers, SBC Technical Books, Atlanta, 1972.

31. Baker, A. J., Rogers, R. C., and Zelazny, S. W., "Analytical Study of Mixing and Reacting Three-Dimensional Supersonic Combustor Flow Fields," in NASA SP-347, 1975.

32. Zelazny, S. W., Baker, A. J. and Rushmore, W. R., "Modeling of Three-Dimensional Mixing and Reacting Ducted Flows," NASA CR- , May 1975.

33. Fearn, Richard and Weston, Robert, "Vorticity Associated with a Jet in a Cross Flow," AIAA J., 12, No. 12, p. 1666-1671, 1974.